Material functions of liquid n -hexadecane under steady shear via nonequilibrium molecular dynamics simulations: Temperature, pressure, and density effects

Huan-Chang Tseng, Jiann-Shing Wu, and Rong-Yeu Chang

Citation: The Journal of Chemical Physics **130**, 084904 (2009); doi: 10.1063/1.3080768
View online: http://dx.doi.org/10.1063/1.3080768
View Table of Contents: http://scitation.aip.org/content/aip/journal/jcp/130/8?ver=pdfcov
Published by the AIP Publishing

Articles you may be interested in

Nonlinearity and slip behavior of n-hexadecane in large amplitude oscillatory shear flow via nonequilibrium molecular dynamic simulation
J. Chem. Phys. **136**, 104904 (2012); 10.1063/1.3693269

Master curves and radial distribution functions for shear dilatancy of liquid n -hexadecane via nonequilibrium molecular dynamics simulations
J. Chem. Phys. **130**, 164515 (2009); 10.1063/1.3123171

Shear thinning and shear dilatancy of liquid n -hexadecane via equilibrium and nonequilibrium molecular dynamics simulations: Temperature, pressure, and density effects
J. Chem. Phys. **129**, 014502 (2008); 10.1063/1.2943314

A comparison of simple rheological models and simulation data of n-hexadecane under shear and elongational flows
J. Rheol. **50**, 625 (2006); 10.1122/1.2240308

Rheological and structural studies of liquid decane, hexadecane, and tetracosane under planar elongational flow using nonequilibrium molecular-dynamics simulations
J. Chem. Phys. **122**, 184906 (2005); 10.1063/1.1897373

This article is copyrighted as indicated in the article. Reuse of AIP content is subject to the terms at: http://scitation.aip.org/termsconditions. Downloaded to IP: 140.113.38.11 On: Wed, 30 Apr 2014 06:13:54

Material functions of liquid *n*-hexadecane under steady shear via nonequilibrium molecular dynamics simulations: Temperature, pressure, and density effects

Huan-Chang Tseng,[1] Jiann-Shing Wu,[1,a)] and Rong-Yeu Chang[2]
[1]*Department of Applied Chemistry, National Chiao Tung University, Hsinchu, Taiwan 30010, Republic of China*
[2]*Department of Chemical Engineering, National Tsing Hua University, Hsinchu, Taiwan 30043, Republic of China*

(Received 30 July 2008; accepted 16 January 2009; published online 26 February 2009)

Computer experiments of rheology regarding the effects of temperature (T), pressure (P), and density (ρ) on steady shear flow material functions, which include viscosity (η) and first and second normal stress coefficients (ψ_1 and ψ_2) depending on shear rate ($\dot{\gamma}$), have been conducted via nonequilibrium molecular dynamics simulations for liquid *n*-hexadecane. Straightforwardly, using both characteristic values of a *zero-shear-rate viscosity* and *critical shear rate*, η-$\dot{\gamma}$ flow curves are well normalized to achieve the temperature-, pressure-, and density-invariant *master curves*, which can be formulary described by the Carreau–Yasuda rheological constitutive equation. Variations in the rate of shear thinning, obviously exhibiting in η-$\dot{\gamma}$, ψ_1-$\dot{\gamma}$, and $-\psi_2$-$\dot{\gamma}$ relationships, under different T, P, and ρ values, are concretely revealed through the power-law model's exponent. More importantly, at low shear rates, the fluid explicitly possesses Newtonian fluidic characteristics according to both manifestations; first and second normal stress differences decay to near zero, while nonequilibrium states are close to equilibrium ones. Significantly, the tendency to vary of the degree of shear thinning in rheology is qualitatively *contrary* to that of shear dilatancy in thermodynamics. In addition, a *convergent transition point* is evidently observed in the $-\psi_2/\psi_1$-$\dot{\gamma}$ curves undergoing *dramatic variations*, which should be associated with shear dilatancy, as addressed analytically. © *2009 American Institute of Physics*. [DOI: 10.1063/1.3080768]

I. INTRODUCTION

Nonequilibrium molecular dynamics (NEMD)[1–3] simulations do provide a valuable tool in academia and industry via microscopic understanding of the observed macroscopic phenomena for rheological properties. At present, most of NEMD applications have been conducted from simple fluid[4,5] to increasingly complex fluids, including *n*-alkane,[6–17] alcohol[18] and ketone[19] molecules, polymer melt,[20–27] water molecules,[19,28] and molten alkali halides,[29,30] as well as organic and polymeric mixture solutions, and blending.[31–35] Such simulations can be employed in both shear and elongation flows,[24,27] which involve both *steady* and *transient* state flow systems.[22,23] Nevertheless, NEMD studies are concentrated mostly in steady state shear flows. Apart from a few noteworthy reports for oscillatory shear flows, both important features of fluids—linear viscoelastic and thermorheological simplistic—have been recently presented using NEMD simulations.[36]

The steady shear material functions[37–39] involve viscosity and first and second normal stress coefficients. In rheology, nonlinear manifestations, such as *shear thinning*, *shear thickening*, and *normal stress differences*, have been commonly observed for polymeric fluids. The first and second normal stress differences are responsible to a variety of significant effects in the polymeric liquid flows, looking for examples[37] of the rod climbing (or Weissenberg), the die swell, the hole-pressure phenomena, and so on. Essentially, Newtonian and non-Newtonian fluids can be recognized by zero and nonzero normal stress differences, respectively.[38]

In early NEMD researches,[4,5] the argon (Ar) fluid at high shear rates possessed both rheological characteristics, namely, shear thinning behavior and nonzero normal stress differences. Also, shear dilatancy of nonequilibrium thermodynamic state, which is related to the shear-rate dependence of pressure or density, was clearly observed. In particular, Heyes[4] and Evans and Morriss[5] inspected that one important issue was the presence of shear thickening, which occurred abruptly at a very extreme shear rate of over 1×10^{13} s^{-1}. This excessive shear rate, however, may be impossibly achieved in the current practical experimental technologies. It obviously shows that the *causes* of non-Newtonian behaviors resulted in NEMD simulations of simple fluids are difficult to understand according to our macroscopic cognition of fluid mechanics. In passing, the experimental results of Ballman[40] indicted surprisingly that the sudden increase in the viscosity of polystyrene melt was examined at a higher shear rate of 7600 s^{-1}.

Up to now, a number of NEMD studies[8,10–13,31] on different state points have analyzed various *n*-alkane molecules, containing linear and branch structures, and have investi-

a)Author to whom correspondence should be addressed. Electronic mail: inblue.ac89g@nctu.edu.tw. Present address: Science Building 2, 1001 Ta Hsueh Road, Hsinchu, Taiwan 30010, Republic of China.

 © 2009 American Institute of Physics

This article is copyrighted as indicated in the article. Reuse of AIP content is subject to the terms at: http://scitation.aip.org/termsconditions. Downloaded to IP: 140.113.38.11 On: Wed, 30 Apr 2014 06:13:54

gated nonequilibrium thermodynamic states and rheological properties, as well as molecular conformations and configurations; thus, those results are also in qualitative agreement with related experimental and theoretical results. Significantly, Bair *et al.*[13] presented evidence of the NEMD simulation data following the same time-temperature superposition master curve[41,42] with experimental data together for squalane fluid. With respect to *n*-hexane/*n*-hexadecane mixture, the concentration dependence of viscosity was achieved by Kioupis and Maginn.[31]

For sheared *alcohol* molecules, Petravic and Delhommelle[18] employed the *optimized potential for liquid simulations* potential mode to describe the *hydrogen bond* interaction; accordingly, their findings at high shear rates emphasized the interrelationship between breaking, stability, and alignment of hydrogen bond and shear thinning. Especially for ionic particles' Coulombic forces described by using an accuracy method of the *Edwald summation*, Galamba *et al.*[30] conducted the NEMD simulation on molten alkali halides including sodium chloride (NaCl) and potassium chloride (KCl). As mentioned above, whether dealing with these various sheared fluids at the molecular level, the relationship between viscosity and shear rate has been invariably presented—the shear thinning behavior at high shear rates.

Regarding NEMD studies on polymer melt, the *finite extensible nonlinear elastic* (FENE) potential[21,43–45] can always coarse grain the chain motion between two beads. From short to long linear chain molecules, Kröger and Hess[21] built the FENE chain motion to analyze the relationship between the zero-shear-rate viscosity (η_0) and the molecular length (N). Consequently, the η_0-N relationship clearly represents a critical chain length characterizing the crossover point from $\eta_0 \propto N^1$ of Roused model to $\eta_0 \propto N^{3.0-3.5}$ of reptation model.[46] In both transient and steady state nonlinear flow[22,23] for shear rates varying from 30 to 3000 μs^{-1} and chain lengths varying from $C_{80}H_{162}$ to $C_{800}H_{1602}$, Padding and Briels[47] investigated rheological data (shear viscosity and normal stress differences) and structural data (chain dimensions and orientation tensor) by using NEMD simulations with a coarse-grained model of polyethylene (PE). Furthermore, Jabbarzadeh *et al.*[25] and Bosko *et al.*[26] clearly presented that the viscosity increases with increasing degree of branches of molecular architecture. In addition, the polymer blending study with respect to linear and branched structures was done by Bosko *et al.*,[34] who pointed out that the percentage of branched polymer chains enhances so that the overall blending viscosity correspondingly increases.

As reviewing the aforementioned NEMD studies, most of attentions worthy are limited with respect to rheological properties, specifically, being related to the molecular intrinsic structures and the blending ratio of branched to linear polymers. According to rheological treatises,[37–39] however, primary factors of induced variations in rheological properties are of course temperature, pressure, and density dependent, as well as molecular structure dependent. Except for the few noteworthy NEMD researches,[11,15] the effects of temperature, pressure, and density on rheological properties have not been examined completely so far.

More recently, we have reported the NEMD discussions[17] of liquid *n*-hexadecane in terms of the variations in shear thinning and shear dilatancy with temperature, pressure, and density. The objective of the present study is to focus on in-deep analyses of rheological properties—the shear-rate ($\dot{\gamma}$) dependence of viscosity (η) and the first and second normal stress coefficients (ψ_1 and ψ_2). These properties varying with different temperatures, pressures, and densities are performed by both *constant volume* NEMD and *constant pressure* NEMD simulations.[1,3,48]

In this present study, Carreau–Yasuda[37,39] rheological constitutive equations of the generalized Newtonian fluid are utilized to describe the overall η-$\dot{\gamma}$ curve, while the η_0 value in the first-Newtonian plateau region is reasonably extrapolated. Furthermore, the *relaxation time* (τ_R) can be assessed by the modified Rouse theory.[7,17,41] The *critical shear rate* ($\dot{\gamma}_c$), which occurred from the first-Newtonian plateau to the shear thinning region, approaches the *inverse* of the relaxation time, namely, $\dot{\gamma}_c \approx \tau_R^{-1}$.[7] Significantly, by selecting both *characteristic* values of η_0 and $\dot{\gamma}_c$ values,[14,35] we can also reduce η-$\dot{\gamma}$ data to obtain temperature-, pressure-, and density-invariant master curves. Even if NEMD simulations have been well established in literature, those master curves have not been extensively discussed so far. Therefore, the master curves obtained from NEMD simulations should be significant, especially for rheological computations.

The shear thinning characteristic not only occurs explicitly at η-$\dot{\gamma}$ curve but also in both ψ_1-$\dot{\gamma}$ and $-\psi_2$-$\dot{\gamma}$ relationships. Simultaneously, the slope of shear thinning can be easily described by the power-law model. Notably, under different temperatures, pressures, and densities, we obtain the qualitative relationship between variations in the degree of shear thinning and shear dilatancy. Moreover, we analytically observe the dramatic variations in $-\psi_2/\psi_1$-$\dot{\gamma}$ curves and their convergent transition (CT) point.

The sections of this present study are organized as follows. In Sec. II, we describe the details of the molecular models, simulation methods, and steady shear material functions. In Sec. III, we reveal the results of rheological properties performed at varying temperatures, pressures, and densities, and compare the results with the earlier related experiments, theories, and NEMD simulations. Overall conclusions and future works are summarized in Sec. IV.

II. SIMULATION DETAILS

In a previous study,[17] we performed NEMD simulations for sheared liquid *n*-hexadecane. For completeness, here we briefly summarize the molecular potential models, simulation methods, and rheological properties in this present study. This section can be split neatly into three parts: the first describes the construction of molecular modeling and potential models, including van der Waals (vdW) and covalent bonding interactions; the second explains equations of motion and their numerical methods used; and the third defines rheological properties, such as stress tensor and material functions, containing viscosity and normal stress coefficients.

This article is copyrighted as indicated in the article. Reuse of AIP content is subject to the terms at: http://scitation.aip.org/termsconditions. Downloaded to IP: 140.113.38.11 On: Wed, 30 Apr 2014 06:13:54

A. Potential models

At the coarse-grained level, a *n*-hexadecane molecular chain is simply modeled using spherical interaction sites, regarded as *methylene* (CH_2) groups. Connected interaction sites will combine together to form molecular chains. This type of molecular chain model is known as the *united atom* (UA). Thus, 1 *n*-hexadecane molecule is approximately consisted of 16 CH_2 groups. The descriptions of chain motions are governed by the vdW interaction and the covalent bonding interaction comprised of bond stretching, bond bending, and torsion motions.

In this present study, the modeling of these molecular motions above is based on the set of realistic potential models of Chynoweth and Michopoulos[9,49] (CM), which only has one UA, CH_2 group. In passing, the transferable potential for phase equilibria (TraPPE) model[50] is an adaptation for calculating the vapor-liquid coexistence curve and the surface tension of *n*-alkane phase diagram. TraPPE model contained two UA groups: CH_2 group and CH_3 group. In a previous study,[17] we have clearly examined both usual CM and TraPPE models for suitability of predicting equilibrium thermodynamic and rheological properties, which are relative to the vapor-liquid coexistence curves and the zero-shear-rate viscosity η_0, respectively.

By using TraPPE model in rheological properties, McCabe *et al.*[51] predicted the η_0 value at different state points for 9-octylheptadecane. As the pressure increases largely, the derivation of their predicted η_0 values and experimental values[52] is increased obviously. Thus, they suggested that TraPPE model's η_0 value was underpredicted, while TraPPE model was parametrized for vapor-liquid equilibria. In addition, Khare *et al.*[10] modified TraPPE model's bond stretching motion by FENE potential; this improved model estimated that the η_0 value of *n*-hexadecane was almost two times larger than the experimental value.[53]

When the CM model was adopted, Chynweth and Michopoulos[9,49] concluded that CM model was suitable in the prediction of rheological properties. Furthermore, Jabbarzadeh *et al.*[54–56] applied the CM model to analyze the rheological properties in *heterogeneous* shear flows. Moreover, for *n*-hexadecane at a state point of 477.6 K and 0.896 g/cm^3, its experimental η_0 value[9,49,52] is 8.34 cP. At the same state point for *n*-hexadecane, our previous study[17] indicted that CM model's η_0 value of 5.39 cP is close to the experimental value and is better than TraPPE model's η_0 value of 3.55 cP.

In summary, when TraPPE model is used in equilibrium thermodynamics, its predicted density of vapor-liquid coexistence curves is close to the related experimental values; correspondingly, when TraPPE model is used in rheological properties, the deviation of its η_0 value with the experimental value is large. On the other hand, CM model predicted that the η_0 value is better, while its predicted density is rather poor. More importantly, no matter which potential model is adopted, the qualitative tendency of simulated physical phenomenon would be similar. Therefore, using CM model in rheological properties is surely more reasonable as compared quantitatively to TraPPE model. Expectedly, we may propose that using TraPPE model to predict the variation in rheological properties is in qualitative agreement with using CM model.

According to the basic viewpoint of quantum chemistry, it is hard to describe molecular orbits and intramolecular interactions (i.e., vdW force, polar bond, and hydrogen bond) by using a simple potential function. The well-known material science computational software—MATERIAL STUDIO—adopts a complex potential function, such as "condensed-phase optimized molecular potentials for atomistic simulation studies (COMPASS)" force field.[57,58] The applications of COMPASS model can perform many predictions, including structural, conformational, vibrational, and thermophysical properties for a broad range of molecules in isolation and in condensed phases and under a wide range of conditions of temperature and pressure. However, no literature has related that this model is able to predict "rheological properties." Therefore, in the MD simulation field, a certain molecular potential model should not be used simultaneously in the predictions of equilibrium thermodynamic and rheological properties, but the confirmation only shows that the simulated physical phenomena are same, whether molecular potential model is used.

For a simple objective, we would relevantly choose CM model in the present study to predict *qualitatively* rheological properties—material functions under steady shear. In addition, we would like to emphasize that the focus is *not* on whether one molecular potential model is better than the other to predict *quantitatively* the rheological properties. Substantially, the primary objective of this present study is to qualitatively present "similar macroscopic rheological experimental results." Thus, those results by NEMD simulations may be helpful for understanding the relationship between microscopic interactions and macroscopic rheological properties, especially for various materials in nanoscale.

The CM model is adopted in the *steady state shear flow*,[17,54–56,59] *oscillatory shear flow*,[36] and *nanocontraction flow*[60] portions of MD simulations. For completeness, we introduce all potential functions for the CM model below and their parameters are listed in Table I.

1. van der Waals interaction

The vdW interaction occurs between CH_2 groups of different chains and also between CH_2 groups in the same chain separated by more than three CH_2 groups. The vdW potential can be described by the 12–6 Lennard-Jones (LJ) potential[9]

$$U_{\mathrm{LJ}} = 4\varepsilon_{\mathrm{LJ}}\left[\left(\frac{\sigma_{\mathrm{LJ}}}{r_{ij}}\right)^{12} - \left(\frac{\sigma_{\mathrm{LJ}}}{r_{ij}}\right)^{6}\right], \tag{1}$$

where r_{ij} is the distance between two CH_2 groups, $\varepsilon_{\mathrm{LJ}}$ and σ_{LJ} are the energy and length parameters of the LJ potential, respectively, for the pair of groups *i* and *j*.

The LJ potential can provide the short-range *repulsion* effect or *excluded volume* effect and long-range *attraction* effect. To reduce computational time of the vdW force, the shifted LJ potential[61] is usually truncated at a cutoff distance r_c (in this present study, r_c=9 Å) so that $U_{\mathrm{LJ}}(r_c)$=0. Thus, physical quantities are of course affected by the LJ potential

This article is copyrighted as indicated in the article. Reuse of AIP content is subject to the terms at: http://scitation.aip.org/termsconditions. Downloaded to IP: 140.113.38.11 On: Wed, 30 Apr 2014 06:13:54

TABLE I. The potential parameters of LJ and covalent bonding interactions.

Parameter		Value[a]	Unit
Lennard-Jones	σ_{LJ}	4.045	Å
	ε_{LJ}	0.420	kJ mol^{-1}
Bond stretching	k_l	2650.98	kJ mol^{-1} Å^{-2}
	l_0	1.53	Å
Bond bending	k_θ	0.1004	kJ mol^{-1} deg^{-2}
	k'_θ	0.0096	deg^{-1}
	θ_0	109.47	deg
Torsion	c_0	9.278	kJ mol^{-1}
	c_1	12.155	kJ mol^{-1}
	c_2	−13.119	kJ mol^{-1}
	c_3	−3.060	kJ mol^{-1}
	c_4	26.239	kJ mol^{-1}
	c_5	−31.493	kJ mol^{-1}

[a]LJ potential parameters (σ_{LJ} and ε_{LJ}) are taken from Ref. 9; equilibrium bond length and bond angle (l_0 and θ_0) are taken from Ref. 49; bond stretching and bond bending force constants (k_l, k_θ, and k'_θ) are taken from Ref. 62; and torsion potential parameters are taken from Ref. 63.

truncation. When the shifted LJ potential is used, long-range corrections must be added to both *internal energy* and *pressure* during the MD simulation procedure.

2. Covalent bonding interaction

The bond stretching potential[62] U_s connects two CH_2 groups by Hooke's harmonic potential with an *equilibrium* bond length l_0 of 1.53 Å,[49]

$$U_s = \tfrac{1}{2}k_l(l_i - l_0)^2, \tag{2}$$

where k_l is the bond stretching energy constant and l_i is the bond length between groups $i-1$ and i.

The bond bending potential[62] U_b is described by the Taylor series' cubic term expansion of bending angle deviation with an *equilibrium* bond angle θ_0 of 109.47°,[49]

$$U_b = \tfrac{1}{2}k_\theta[(\theta_i - \theta_0)^2 - k'_\theta(\theta_i - \theta_0)^3], \tag{3}$$

where k_θ is the bond bending energy constant, k'_θ is the bond bending angle constant, and θ_i is a bond angle among three adjacent CH_2 groups $i-1$, i, and $i+1$.

The torsion potential[63] U_t is expressed by a fifth-order cosine polynomial of a dihedral angle,

$$U_t = c_0 + c_1\cos\phi_i + c_2\cos^2\phi_i + c_3\cos^3\phi_i + c_4\cos^4\phi_i + c_5\cos^5\phi_i, \tag{4}$$

where $\{c_n\}$ are the values of the set of torsion energy coefficients and ϕ_i is the dihedral angle formed by four consecutive CH_2 groups $i-1$, i, $i+1$, and $i+2$. There are three stable minima in U_t. The lowest energy state is the *trans* conformation at $\phi_i=0°$ or $\phi_i=360°$. The other two stable states are *gauche* conformations, g^+ and g^-, located at $\phi_i=\pm 120°$, respectively. The *cis* state, at $\phi_i=180°$, has very high and unstable energy.[64]

B. Simulation algorithms

The NEMD algorithm[1,3,48] was originally developed by combining SLLOD (Ref. 65) equations of motion with the Lees–Edwards sliding brick periodic boundary condition.[66] In this present study, we performed the NEMD simulations under isothermal conditions involving both constant volume NEMD (*NVT*-NEMD) and constant-pressure[67,68] NEMD (*NPT*-NEMD) systems. The flow (x-axis) and gradient (y-axis) directional sizes (L_x and L_y, respectively) of the simple shear flow system were 3.0 and 4.5 nm, respectively. A shear rate $\dot\gamma$ was applied to the fluid to characterize the shear flow field; $\dot\gamma$ is related to the streaming velocity v_x in the x direction, namely, $\dot\gamma=\partial v_x/\partial y$. The *periodic boundary condition*[1,61] was adopted in *all* directions, while the Lees–Edwards boundary condition[1,66] was used in the xy plane.

Significantly, for a system of rigid homonuclear *diatomic molecules* undergoing planar Couette flow, Travis *et al.*[69,70] recently demonstrated that molecular stress tensor can contain a *nonvanishing antisymmetric* component due to unintentional body torques of molecular architecture occurring via an atomic thermostat.[17] Thereby, their results presented that both thermostating schemes differ in their viscosity-shear-rate relationship, especially for high shear rate (reduced shear rate $\geq$2.5).[25] In contrast to low shear rates, the same results are produced essentially for both thermostating schemes.

In the present study, both *NVT*-NEMD and *NPT*-NEMD simulations choose the atomic version under constant shear rate, including the SLLOD equations of motion, temperature, and stress tensor to result in no strange effects on the predicted rheological properties for $\dot\gamma < 1.1\times10^{12}$ s^{-1} (below 2.5 in reduced units of shear rates).[25] Most of NEMD simulations[10,13,22,56,71] at shear rates over 1×10^8 s^{-1} are extreme shear rate studies in contrast to the typical macroscopic experiments of shear flow. For modern tribology in automobile engines, such as disk drives, micromachines, and camshaft lifters,[71] however, an extreme shear rate in the thickness of lubrication film about 5 nm (quite ten molecularly lays)[56,72] and as high as 1×10^8 s^{-1} may be expected. Hence, some high shear rates should be accessibly imposed to analyze computationally rheological properties in ultrathin films of industrial lubrications.

In addition, the SLLOD equations of motion can be implemented by the leapfrog-Verlet scheme of MacGowan and Heyes[73] which offers a fast converging *iterative* algorithm for Gaussian thermostat multiples.[7] The magnitude of time step depends on a shear rate from 1.0 to 0.1 fs due to ensuring numerical stability.[17] Detailed information above regarding the molecular potentials, the SLLOD algorithms, and other related methods is available elsewhere.[17]

C. Rheological properties

Under the steady shear, the standard material functions of fluids contain viscosity and first and second normal stress coefficients. All of the functions depend on the atomic stress tensor and shear rate below. Note that the atomic stress tensor is characterized from the trajectories obtained in the NEMD simulation procedure.

1. Atomic stress tensor

In a homogenous system volume V, the atomic stress tensor is given by the Irving–Kirkwood's equation[1,74]

This article is copyrighted as indicated in the article. Reuse of AIP content is subject to the terms at: http://scitation.aip.org/termsconditions. Downloaded to IP: 140.113.38.11 On: Wed, 30 Apr 2014 06:13:54

$$\tau_{\alpha\beta} = -\frac{1}{V}\left(\sum_{i=1}^{N}\frac{p_{i\alpha}p_{i\beta}}{m_i} + \sum_{i=1}^{N}\sum_{j>i}^{N} r_{ij\alpha}f_{ij\beta}\right), \tag{5}$$

where $\tau_{\alpha\beta}$ is a component of the stress tensor, subscripts $\alpha,\beta=x,y,z$, $\mathbf{p}_i$ is the peculiar momentum of the ith atom, p_{xi} and p_{yi} are components of $\mathbf{p}_i$, m_i is the mass of the ith atom, r_{ij} denotes the distance vector from atom j to atom i, f_{ij} denotes the force imposed on atom i due to atom j, and N equals the total number of atoms. On the right side of Eq. (5), the *first* sum describes the contribution of the kinetic energy, and the *second* sum describes the contribution of virial energy.[1] The force term f_{ij} consists of both vdW interaction and covalent bonding interactions, which contain the bond stretching, bond bending, and torsion motions. The expressions of these forces' Virial energy were briefly described in the stress tensor study of Carpenter.[75]

2. Viscosity and normal stress coefficients

In the steady state shear flow field, the viscosity of fluids is defined by[37–39]

$$\eta = \frac{\tau_{yx}}{\dot{\gamma}}, \tag{6}$$

where τ_{yx} is the yx component of the stress tensor. The traditional log η versus log $\dot{\gamma}$ curve is called the *flow curve*, including both features—the first-Newtonian plateau and the shear thinning slope. The first-Newtonian plateau regime indicates that as the shear rate approaches zero, all fluids exhibit Newtonian behavior, which allows the determination of the zero-shear-rate viscosity, η_0, i.e., $\eta_0=\lim_{\dot{\gamma}\to 0}\eta(\dot{\gamma})$. At high shear rates, the shear thinning regime is described to be linear relationship between log η and log $\dot{\gamma}$ by power-law model, $\eta \propto \dot{\gamma}^{-k}$, where k is an exponent.

The first and second normal stress coefficients ψ_1 and ψ_2 are obtained from[37–39]

$$\psi_1 = \frac{N_1}{\dot{\gamma}^2} = \frac{\tau_{xx}-\tau_{yy}}{\dot{\gamma}^2}, \tag{7}$$

$$\psi_2 = \frac{N_2}{\dot{\gamma}^2} = \frac{\tau_{yy}-\tau_{zz}}{\dot{\gamma}^2}, \tag{8}$$

where N_1 and N_2 are the first and second normal stress differences, respectively. Experimentally, for polymeric fluids, ψ_2 is a negative value with a magnitude of about *one-tenth* ψ_1, $\psi_2 \approx -\frac{1}{10}\psi_1$. As for the zero-shear-rate limit, $\psi_{1,0}=\lim_{\dot{\gamma}\to 0}\psi_1(\dot{\gamma})$ and $\psi_{2,0}=\lim_{\dot{\gamma}\to 0}\psi_2(\dot{\gamma})$. On the logarithmic coordinate, ψ_1 and $-\psi_2$ at high shear rates are plotted as a *linear* function of shear rate, namely, $\psi_1 \propto \dot{\gamma}^{-\alpha}$ and $-\psi_2 \propto \dot{\gamma}^{-\beta}$, where exponents α and β can quantify the slope of shear thinning.

III. RESULTS AND DISCUSSION

In a homogenous steady shear flow field, the rheological properties of liquid n-hexadecane including the dependence of viscosity (η) and first and second normal stress coefficients (ψ_1 and ψ_2) on shear rate ($\dot{\gamma}$) are analyzed in detail as follows. First, Sec. III A clearly illustrates that the shear thinning feature described by using power-law model[37,39] not only presents in η-$\dot{\gamma}$ curves but also appears in both ψ_1-$\dot{\gamma}$ and $-\psi_2$-$\dot{\gamma}$ relationships; then, these results are compared with related NEMD simulations, experiments, and theories. Second, in Sec. III B one of the main objective of the present study is to further perform η-$\dot{\gamma}$ flow curves normalized to gain three master curves with respect to temperature, pressure, and density invariant, when based on our earlier results.[17] Also, master curves are well formulated by using the Carreau–Yasuda rheological model.[37,39] Lastly, in Sec. III C another goal of the present study is to observe how first and second normal stress differences and coefficients change in relation to the effects of temperature, pressure, and density; significantly, we discuss variations in the rate of shear thinning in detail. Accordingly, as compared qualitatively, the degree of shear thinning in rheology is related to that of shear dilatancy in thermodynamics.

A. Validity of normal stress coefficients

Regarding non-Newtonian fluid, its η-$\dot{\gamma}$ flow curve consists of two regions, namely, the zero-shear-rate viscosity (η_0) in first-Newtonian plateau region and the slope of shear thinning in non-Newtonian region. In our earlier study,[17] we have offered valid evidences with respect to the η-$\dot{\gamma}$ flow curves in both constant volume NEMD (*NVT*-NEMD) and constant pressure NEMD (*NPT*-NEMD) simulations. These results are in agreement with the previous related studies including NEMD simulations, experiments, and theories.

Here, the *NVT*-NEMD simulation system of the present study, which is a rectangular three-dimensional box with $L_x=3.0$ nm, $L_y=4.5$ nm, and $L_z=4.5$ nm, contains 144 n-hexadecane molecules at a state point of 477.6 K and 0.896 g/cm^3. The n-hexadecane fluid is surely of a liquid state at this state point since its melting and boiling points are at about 291.3 K (Ref. 76) and 560 K,[9] respectively. The x and y directions of the system box correspond to flow and gradient directions, respectively. Significantly, we focus on the $\dot{\gamma}$ dependence of ψ_1, ψ_2, and $-\psi_1/\psi_2$ on the following.

In rheological experiments, measuring the ψ_1 and ψ_2 values is not easily obtained. For polymeric liquid, ψ_1 is a positive value, and ψ_2 is a negative value which is about one-tenth magnitude of ψ_1. Notably, to represent on logarithmic coordinates together with ψ_1, ψ_2 must add a minus sign, i.e., $-\psi_2$.[37–39] As shown in Fig. 1 over a wide shear range of $1\times10^{9.5}-1\times10^{12.5}$ s^{-1}, both results are in accordance with those characteristics above of ψ_1 and $-\psi_2$ and are also in close agreement with the results of Chynoweth *et al.*[49] In this present study, the shear rate is least limited at $1\times10^{9.5}$ s^{-1} due to the fact that lower shear rates generate the lower signal-to-noise ratio producing large statistical errors.[10] Obviously, between $1\times10^{10.0}$ and $1\times10^{12.0}$ s^{-1} the ψ_1-$\dot{\gamma}$ and $-\psi_2$-$\dot{\gamma}$ curves are close to the linear line in the logarithmic plot. This is one representation of shear thinning. In contrast to $\dot{\gamma}<1\times10^{10.0}$ s^{-1}, both curves start deviating from the slope of shear thinning.

Additionally, both curves are fit via the power-law model, namely, $\psi_1 \propto \dot{\gamma}^{-\alpha}$ and $-\psi_2 \propto \dot{\gamma}^{-\beta}$, where $\alpha=1.42$ and $\beta=1.38$ in Fig. 1. Early NEMD study of Edberg *et al.*[6] re-

This article is copyrighted as indicated in the article. Reuse of AIP content is subject to the terms at: http://scitation.aip.org/termsconditions. Downloaded to IP: 140.113.38.11 On: Wed, 30 Apr 2014 06:13:54

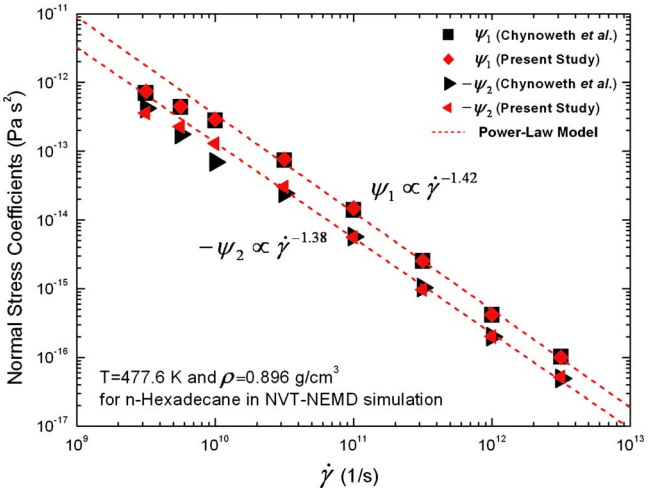

FIG. 1. (Color online) Shear-rate $\dot{\gamma}$ dependence on the first normal stress coefficient ψ_1 and the minus second stress coefficient $-\psi_2$ for *n*-hexadecane at 477.6 K and 0.896 g/cm^3 as obtained from *NVT*-NEMD simulation.

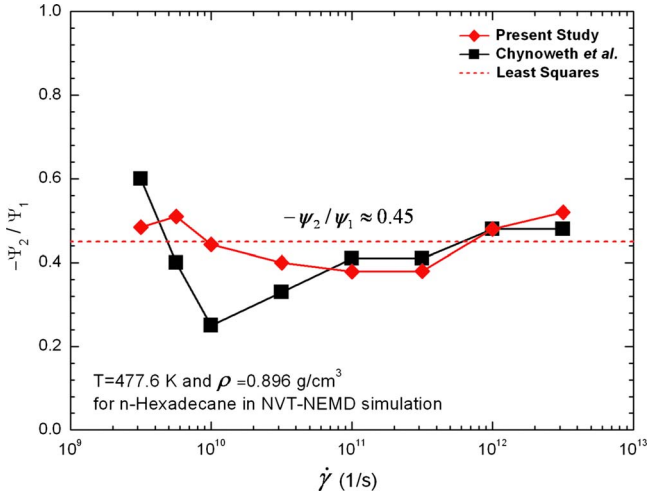

FIG. 2. (Color online) Shear-rate $\dot{\gamma}$ dependence on the minus ratio of the second to first normal stress coefficient $-\psi_2/\psi_1$ for *n*-hexadecane at 477.6 K and 0.896 g/cm^3 as obtained from *NVT*-NEMD simulation.

garding *n*-butane (C_4H_{10}) and *n*-decane ($C_{10}H_{22}$) fluids have shown $\psi_1 \propto \dot{\gamma}^{-1.5}$ and $-\psi_2 \propto \dot{\gamma}^{-1.5}$. Khare *et al.*[10] suggested $\psi_1 \propto \dot{\gamma}^{-(1.30-1.45)}$ for a wide various *n*-alkane molecules. Incidentally, in the molecular theory with regard to entangled polymer dynamics, the Doi–Edwards model predicted $\psi_1 \propto \dot{\gamma}^{-2.0}$ and $-\psi_2 \propto \dot{\gamma}^{-2.5}$ as $\dot{\gamma} \to \infty$.[22,23,46] For long molecular chains consisting of 100–400 beads, NEMD results of Aoyagi and Doi[20] revealed $\psi_1 \propto \dot{\gamma}^{-1.5}$ and $-\psi_2 \propto \dot{\gamma}^{-1.8}$, which are in close agreement with the theory[46] of polymer dynamics.

In the ensuing discussion of shear thinning, as for our earlier study,[17] the η-$\dot{\gamma}$ curves on the logarithmic coordinate between $1\times10^{10.0}$ and $1\times10^{12.0}$ s^{-1} is also a linear tendency. The slope of shear thinning can be also depicted by the power-law model, namely, $\eta \propto \dot{\gamma}^{-k}$, where k is an exponent. This exponent k is 0.47, which falls reasonably within the range of 0.4–0.9 often reported for the treatise[37] of polymeric liquid. In NEMD results of Khare *et al.*,[10] for varied *n*-alkane molecules, the k value is about 0.37–0.43. Especially in regard to the theory of entangled polymer dynamics, the Doi–Edwards model predicted $\eta \propto \dot{\gamma}^{-1.5}$ as $\dot{\gamma} \to \infty$.[22,23,46] Although molecule lengths and state points are somewhat different, our predicted power-law model's exponents including k (0.47), α (1.42), and β (1.38) for $\eta \propto \dot{\gamma}^{-k}$, $\psi_1 \propto \dot{\gamma}^{-\alpha}$, and $-\psi_2 \propto \dot{\gamma}^{-\beta}$ are reasonable values in comparison with the related studies mentioned above, respectively.

Eventually, the $-\psi_1/\psi_2$ ratio in general is unchanged with shear rate and is about 0.1–0.3 according to the related polymer rheological treatises.[37–39] In the theory of polymer dynamics, for a high shear rate of $\dot{\gamma} \approx 4.3\times10^{11.0}$ s^{-1}, the Doi–Edwards model had derived $-\psi_1/\psi_2 = 2/7 \approx 0.3$.[46] In the present study, Fig. 2 shows that $-\psi_1/\psi_2$ versus $\dot{\gamma}$ is made a constant function via least-squares fitting,[7] which is indicted by the horizontal dashed line; then, our $-\psi_1/\psi_2$ ratio of least-squares fitting for liquid *n*-hexadecane is about 0.45 and is larger than that of polymeric liquid of 0.3. As compared with the result of Chynoweth *et al.*,[49] we present that the change in $-\psi_1/\psi_2$ with $\dot{\gamma}$ does not evidently result in the *fluctuant* tendency at lower shear rates due to our numerical convergence requiring long computational time. Especially for short-chain PE consisting of 100 repeat units, Moore *et al.*[22] concluded that the $-\psi_1/\psi_2$ ratio approaches a value of 0.19. As the $-\psi_1/\psi_2$ ratio of Khare *et al.*[10] is about 0.4–0.5 for various liquid *n*-alkanes, our predicted $-\psi_1/\psi_2 \approx 0.45$ for *n*-hexadecane is a rather acceptable value.

In summary, *n*-hexadecane molecules related to polymer chain are quite short and should be properly considered as the Newtonian fluid in macroscopic perspective. As corroborated above, liquid *n*-hexadecane at the molecular level obviously represents rheological characteristics of polymeric fluids, namely, shear thinning behavior.

B. Master curves of viscosity-shear-rate relationship

With various thermodynamics states (temperature-pressure-density data), the changes in viscosity are noticeably sensitive.[37,39] In our earlier study,[17] using Doolittle's *free volume concept*[42] cooperated with our data of nonthermodynamic state, we have attempted to explain qualitatively the variations in viscosity with respect to the temperature, pressure, and density. While based on our earlier study,[17] here, it is significant that all η-$\dot{\gamma}$ curves are normalized to obtain separately temperature-, pressure- and density-invariant master curves via both *characteristic* values—zero-shear-rate viscosity and critical shear rate.[41] Also, these master curves can be well formulated by the Carreau–Yasuda rheological constitutive equation.[37,39]

1. Temperature-invariant master curve

As a beginning, we use *NPT*-NEMD simulations at a constant pressure of 250 MPa for liquid *n*-hexadecane and the variations in η-$\dot{\gamma}$ flow curves occur at five different temperatures of 300, 350, 400, 450, and 500 K. Substantially, the melting point and boiling point of *n*-hexadecane are 291.3 K (Ref. 76) and 558 K,[9] respectively. The fluid between 300 and 500 K is surely of a liquid state. This result has been represented in our earlier study.[17] Doolittle's free volume concept[42] is often useful in explaining the variations in vis-

This article is copyrighted as indicated in the article. Reuse of AIP content is subject to the terms at: http://scitation.aip.org/termsconditions. Downloaded to IP: 140.113.38.11 On: Wed, 30 Apr 2014 06:13:54

TABLE II. The temperature dependence of various rheological properties at 250 MPa in *NPT*-NEMD simulation.

	T				
	300 K	350 K	400 K	450 K	500 K
η_0 (mPa s)	8.253	4.215	2.637	1.905	1.363
ρ_e (g/cm^3)[a]	0.836	0.818	0.801	0.785	0.770
τ_R (ps)	543.7	243.2	136.0	89.1	58.5
$\dot{\gamma}_c$ (s^{-1})	1.8×10^9	4.1×10^9	7.4×10^9	1.1×10^{10}	1.7×10^{10}
k[a]	0.585	0.541	0.499	0.457	0.412
α	1.609	1.546	1.489	1.420	1.368
β	1.578	1.503	1.452	1.386	1.331

[a]Taken from Ref. 17.

cosity with thermodynamic state: as the free volume of the fluid's molecules increases, its viscosity falls. As for our earlier result,[17] it is evident that density decreases with rising temperature so that the free volume is also enhanced. From a molecular aspect, a decrease in the viscosity is the presentation of the increasing mobility or decreasing resistance to molecular motion; thus, the viscosity decreases with increasing free volume.[17]

With respect to gaining the extrapolative zero-shear-rate viscosity η_0 values, first, we use the Carreau–Yasuda equation here[37,39] to fit η-$\dot{\gamma}$ data of our earlier study,[17]

$$\eta = \eta_\infty + \frac{\eta_0 - \eta_\infty}{[1+(\lambda\dot{\gamma})^a]^{(n-1)/a}}. \tag{9}$$

The Carreau–Yasuda equation has five parameters: η_0 is the very low shear-rate viscosity, i.e., zero-shear-rate viscosity; η_∞ is the very high shear-rate viscosity; λ is the dimension of time; a and n are the exponents; a affects the curvature of the transition region between the first-Newtonian plateau and shear thinning slope; and n controls the slope of the shear thinning region.[39] In general, $\eta_\infty=0$ and $a=2$ are set to reduce the Carreau–Yasuda model for liquid polymeric fluids.[37] Notably, as shown in our previous study,[17] the very high shear-rate viscosity is constrained to zero, i.e., $\eta_\infty=0$, due to no second-Newtonian viscosity appearing in the shear thinning region between $1\times10^{10.0}$ and $1\times10^{12.0}$ s^{-1}.

Next, the rotational relaxation time τ_R is calculated by the modified Rouse model[7,17,41] with the known extrapolative η_0 value above,

$$\tau_R = \frac{6\eta_0 M}{\pi^2 \rho_e RT}, \tag{10}$$

where M is the molecular weight and ρ_e is the equilibrium density. In addition, a *critical shear rate* γ_c indicates an onset point of shear thinning. Berker *et al.*[7] found that $\gamma_c \approx \tau_R^{-1}$, which is in close agreement with the observed NEMD simulation data. Lastly, η_0, ρ_e, τ_R, and $\dot{\gamma}_c$ values at different temperatures are arranged in Table II. As a result, η_0 and τ_R values decrease with rising temperature. Subsequently, the slope of shear thinning can be described by the power-law model, $\eta \propto \dot{\gamma}^{-k}$, where k is the power-law model's exponent and implicitly indicates "the rate or degree of shear thinning." The temperature dependence of the k value is also listed in Table II; thus, the rate of shear thinning falls with rising temperature. These results are also consistent with the general physical understanding of polymers. The power-law model's exponent k of $\eta \propto \dot{\gamma}^{-k}$ will be discussed together with that of $\psi_1 \propto \dot{\gamma}^{-\alpha}$ and $-\psi_2 \propto \dot{\gamma}^{-\beta}$ in Sec. III B 2.

To obtain a temperature-invariant master curve, η-$\dot{\gamma}$ flow curves at different temperature are always normalized via both characteristic values of η_0 and $\dot{\gamma}_c$ according to the treatises[37,41] of polymer viscoelasticity and rheology. In related NEMD simulations, Moore *et al.*[12] and Kairn *et al.*[35] also adopted η_0 and $\dot{\gamma}_c$ values to normalize η-$\dot{\gamma}$ curves at different state points. In addition, the normalized η-$\dot{\gamma}$ curves of MaCabe *et al.*[14] are performed by choosing a scale factor Z in the η/Z versus $\dot{\gamma}Z$ diagram, where $Z=\eta/\eta_{\text{ref}}$ and η_{ref} is the reference viscosity. In particular, employing the time-temperature superposition,[42] an important finding of Bair *et al.*[13] is presented in which the NEMD and experimental data follow the same master curve, together.

Therefore, at five different temperatures of 300–500 K, we also attempted to normalize η-$\dot{\gamma}$ curves to result in a temperature-invariant master curve by adopting η_0 and τ_R values, which are listed in Table II. As a result, η and $\dot{\gamma}$ values are reduced to η/η_0 and $\dot{\gamma}/\dot{\gamma}_c$, respectively. As expected in Fig. 3, almost all η/η_0-$\dot{\gamma}/\dot{\gamma}_c$ points exhibit a very narrow bandwidth; further, the *normalized* Carreau–Yasuda

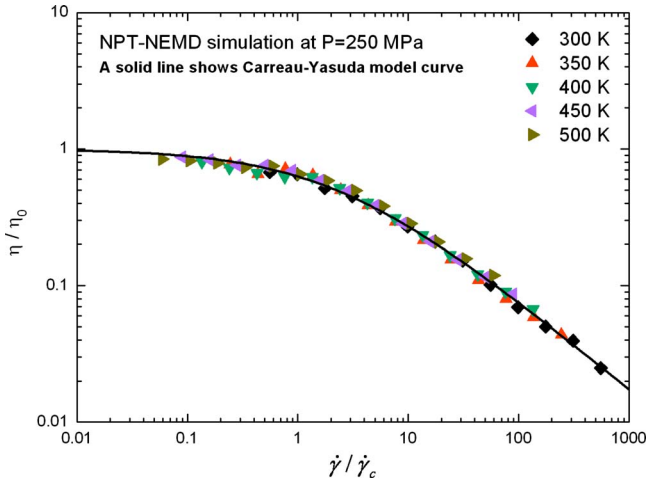

FIG. 3. (Color online) Temperature-invariant master curve of the reduced viscosity η/η_0 vs reduced shear rate $\dot{\gamma}/\dot{\gamma}_c$ for *n*-hexadecane at 250 MPa between 300 and 500 K as obtained from *NPT*-NEMD simulation. The solid line is the Carreau–Yasuda model curve fit to the data.

This article is copyrighted as indicated in the article. Reuse of AIP content is subject to the terms at: http://scitation.aip.org/termsconditions. Downloaded to IP: 140.113.38.11 On: Wed, 30 Apr 2014 06:13:54

TABLE III. The pressure dependence of various rheological properties at 400 K in NPT-NEMD simulation.

	P					
	50 MPa	100 MPa	250 MPa	500 MPa	750 MPa	1000 MPa
η_0 (mPa s)	1.102	1.424	2.637	7.835	⋯	⋯
ρ_e (g/cm^3)[a]	0.699	0.737	0.801	0.866	⋯	⋯
τ_R (ps)	65.1	79.8	136.0	373.9	⋯	⋯
$\dot{\gamma}_c$ (s^{-1})	1.5×10^{10}	1.3×10^{10}	7.4×10^{9}	2.7×10^{9}	⋯	⋯
k [a]	0.449	0.459	0.499	0.542	0.578	0.612
α	1.415	1.433	1.489	1.558	1.611	1.671
β	1.369	1.391	1.452	1.524	1.559	1.601

[a]Taken from Ref. 17.

model to well fit these reduced points is used,

$$\eta^* = \eta_\infty^* + \frac{\eta_0^* - \eta_\infty^*}{[1+(\lambda^*\dot{\gamma}^*)^a]^{(n-1)/a}}, \tag{11}$$

where $\eta^*=\eta/\eta_0$, $\eta_0^*=\eta_0/\eta_0$, $\eta_\infty^*=\eta_\infty/\eta_0$, $\lambda^*=\lambda\dot{\gamma}_c$, and $\dot{\gamma}^*=\dot{\gamma}/\dot{\gamma}_c$. Successfully, we can formulate the reduced $\eta/\eta_0-\dot{\gamma}/\dot{\gamma}_c$ data to obtain the temperature-invariant master curve of the normalized Carreau–Yasuda model with its parameters, i.e., $\eta_0^*=1$, $\eta_\infty^*=0$, $\lambda^*=0.142$, $a=0.53$, and $n=0.10$, as seen in Fig. 3.

2. Pressure-invariant master curve

Over a wide pressure region between 50 and 1000 MPa, using *NPT*-NEMD simulations, the variations in the η-$\dot{\gamma}$ curves are discussed for liquid *n*-hexadecane at a constant temperature of 400 K. Our previous study[17] has represented this illustration, which indicated evidently that viscosity increases with pressure. As a result, only at four different pressures of 50, 100, 250, and 500 MPa, the curves opposes a Newtonian plateau following shear thinning region; other curves only has a shear thinning characteristic. Explained by Doolittle's free volume concept, the effect of increased density and decreased free volume signify that viscosity is enhanced with pressure; thus, this result is in agreement with general rheological understanding.

Referring to Sec. III B 1, η-$\dot{\gamma}$ flow curves at four different pressures (50–500 MPa) in our earlier study[17] are fit via the Carreau–Yasuda model of Eq. (9) to extrapolate η_0 value; further, using the modified Rouse model of Eq. (10) and η_0 value, τ_R can be determined while $\dot{\gamma}_c$ approaches τ_R^{-1}, where the modified Rouse model needs the ρ_e value. Thereby, the η_0, ρ_e, τ_R, and $\dot{\gamma}_c$ values are arranged together in Table III. As expected, η_0 and τ_R values increase with pressure; this tendency is consistent with the general physical understanding of polymers. Moreover, the slopes of shear thinning between $1\times10^{10.0}$ and $1\times10^{12.0}$ s^{-1} at different pressures can be easily described by the power-law model, $\eta\propto\dot{\gamma}^{-k}$, where k is an exponent and implies the rate of shear thinning. Furthermore, the pressure against the exponent is listed in Table III; then, with rising pressure, the rate of shear thinning enhanced is in accordance with common rheological perception.

Eventually, η-$\dot{\gamma}$ curves possess zero-shear-rate viscosities only at four different pressures of 50, 100, 250, and 500 MPa. As in Sec. III B 1, we can also normalize these flow curves to gain one pressure-invariant master curve by adopting η_0 and $\dot{\gamma}_c$ values which the data are obtained in Table III; then, the normalized plot of η/η_0 against $\dot{\gamma}/\dot{\gamma}_c$ is depicted in Fig. 4. Expectedly, all η/η_0-$\dot{\gamma}/\dot{\gamma}_c$ points also present a very narrow bandwidth; those points can be fitted using the normalized Carreau–Yasuda model of Eq. (11) again, where a controlling curvature at the transition point is held constant at 0.53 ($a=0.53$) and is the same with temperature effect. Thus, the pressure-invariant master curve is well described by the normalized Carreau–Yasuda model with its parameters: $\eta_0^*=1$, $\eta_\infty^*=0$, $\lambda^*=0.217$, $a=0.53$, and $n=0.20$, as seen in Fig. 4.

3. Density-invariant master curve

In a liquid-vapor coexistence curve of *n*-hexadecane molecules, the observation of phase diagram at 400 K shows the liquid state at density of over 0.65 g/cm^3; in contrast to below 0.65 g/cm^3, the fluid exhibits the coexistence of liquid and vapor states. This result is referred to in our previous study.[17] To ensure that our simulated fluid is well within the one liquid phase region, therefore, in the present study for NEMD simulation at a constant temperature of 400 K, five different densities of *n*-hexadecane fluid can be surely set at 0.70, 0.75, 0.80, 0.85, and 0.90 g/cm^3.

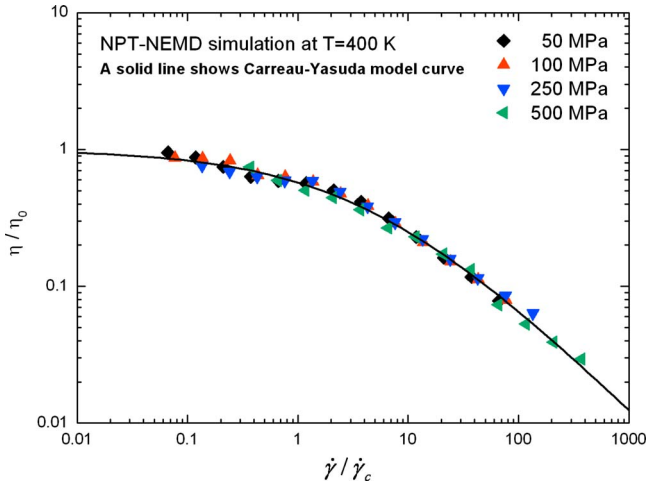

FIG. 4. (Color online) Pressure-invariant master curve of the reduced viscosity η/η_0 vs reduced shear rate $\dot{\gamma}/\dot{\gamma}_c$ for *n*-hexadecane at 400 K between 50 and 500 MPa as obtained from *NPT*-NEMD simulation. The solid line is the Carreau–Yasuda model curve fit to the data.

This article is copyrighted as indicated in the article. Reuse of AIP content is subject to the terms at: http://scitation.aip.org/termsconditions. Downloaded to IP: 140.113.38.11 On: Wed, 30 Apr 2014 06:13:54

TABLE IV. The density dependence of various rheological properties at 400 K in *NVT*-NEMD simulation.

	ρ				
	0.70 g/cm^3	0.75 g/cm^3	0.80 g/cm^3	0.85 g/cm^3	0.90 g/cm^3
η_0 (mPa s)	0.814	1.278	⋯	⋯	⋯
τ_R (ps)	48.0	70.4	⋯	⋯	⋯
$\dot{\gamma}_c$ (s^{-1})	2.1×10^{10}	1.4×10^{10}	⋯	⋯	⋯
k[a]	0.278	0.332	0.392	0.449	0.505
α	1.179	1.295	1.388	1.486	1.580
β	1.128	1.229	1.315	1.385	1.473

[a]Taken from Ref. 17.

At five different densities above, we observe the variation in the η-$\dot{\gamma}$ flow curves by using *NVT*-NEMD simulation of liquid *n*-hexadecane at a constant temperature of 400 K. This representation of η-$\dot{\gamma}$ curves has been shown in our earlier study.[17] Notably, between 0.70 and 0.75 g/cm^3, the η-$\dot{\gamma}$ flow curves are from the first-Newtonian plateau following the slope of shear thinning. With density increasing slightly, the Newtonian regime's scope decreased rapidly. As the density approached 0.80 g/cm^3, the Newtonian regime's scope almost vanished. At higher densities of 0.85 and 0.90 g/cm^3, no sign of the Newtonian plateau exhibits in the η-$\dot{\gamma}$ flow curves. In addition, there is an incremental increase in viscosity at increased density. According to Doolittle's free volume concept, the increase in density results in a decrease in the free volume of molecules.[17]

The Carreau–Yasuda model also can be used to fit the overall η-$\dot{\gamma}$ flow curves at 0.70 and 0.75 g/cm^3 in our earlier study.[17] The same as the discussions in Secs. III B 1 and III B 2, at different densities, all related rheological properties including the η_0, τ_R, and $\dot{\gamma}_c$ values are listed in Table IV. As a result, η_0 and τ_R values increase with density that is qualitatively consistent with the physical perspective of polymers. In addition, the slopes of shear thinning between $1\times10^{10.0}$ and $1\times10^{12.0}$ s^{-1} at all different densities can be obtained by power-law model fitting to η-$\dot{\gamma}$ data, where the power-law model's exponent with respect to the density also is arranged in Table IV.

As the density increased, the rate of shear thinning enhances. This tendency is the same with the effect of pressure. Notably, the variation ranges of the exponent in Tables III and IV are 0.449–0.612 at a pressure interval of 50–1000 MPa and 0.278–0.505 at a density interval of 0.70–0.90 g/cm^3, respectively. Comparably, the rate of shear thinning enhanced with *slightly* increasing density is more sensitive than that with the incremental increase in pressure. Noteworthily, with varying temperatures, pressures, and densities, we perceive that variations in the degree of shear thinning in rheology is qualitatively contrary to that of shear dilatancy in thermodynamics, according to those exponents mentioned above and the data of shear dilatancy of our earlier study.[17]

In a constant shear-rate region of $1\times10^{9.0}-1\times10^{12.0}$ s^{-1}, η-$\dot{\gamma}$ flow curve only at 0.70 and 0.75 g/cm^3 has the η_0 value, while both curves can be normalized by the η_0 and $\dot{\gamma}_c$ values, again. Expectedly, in Fig. 5 almost all reduced points (η/η_0 and $\dot{\gamma}/\dot{\gamma}_c$) show a very narrow bandwidth which is formulated by the normalized Carreau–Yasuda model, where a is also held constant at 0.53 ($a=0.53$) and is the same with the effects of temperature and pressure. Consequently, Carreau–Yasuda model parameters are $\eta_0^*=1$, $\eta_\infty^*=0$, $\lambda^*=1.151$, $a=0.53$, and $n=0.58$. As shown in Fig. 5, the η/η_0-$\dot{\gamma}/\dot{\gamma}_c$ data own the density-invariant master curve.

In particular, what needs to be remarked regarding the variation sensitivity of the η-$\dot{\gamma}$ flow curves which are influenced by the effects of temperature, pressure, and density, is an order of these effects. In our earlier study,[17] the change in shape of η-$\dot{\gamma}$ flow curves are simply observed at different temperatures, pressures, and densities, respectively. As a result, we cautiously inspect in a qualitative comparison concerning the order of sensitizer: the strongest is density effect, the second is pressure effect, and the weakest is temperature effect.

Finally, for temperature-, pressure-, and density-invariant master curves, we have tabulated all of the parameters of the Carreau–Yasuda model in Table V, where η_0^*, η_∞^*, and a are held constant to be 1.0, 0.0, and 0.53, respectively. Furthermore, λ^* and n parameters, which imply the molecular chain's relaxation time and the slope of shear thinning, respectively, are quantitatively compared. Accordingly, the order of the sensitivity, which describes the degree of the variation in η-$\dot{\gamma}$ flow curves with temperature, pressure, and

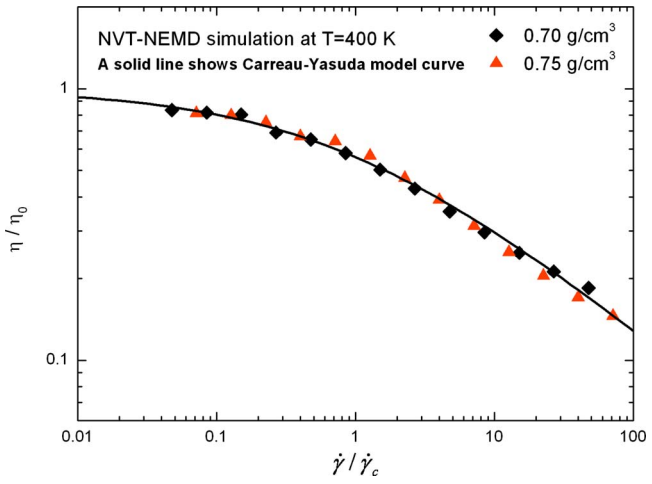

FIG. 5. (Color online) Density-invariant master curve of the reduced viscosity η/η_0 vs reduced shear rate $\dot{\gamma}/\dot{\gamma}_c$ for *n*-hexadecane at 400 K between 0.70 and 0.75 g/cm^3 as obtained from *NVT*-NEMD simulation. The solid line is the Carreau–Yasuda model curve fit to the data.

This article is copyrighted as indicated in the article. Reuse of AIP content is subject to the terms at: http://scitation.aip.org/termsconditions. Downloaded to IP: 140.113.38.11 On: Wed, 30 Apr 2014 06:13:54

TABLE V. The five parameters of the Carreau–Yasuda rheological constitutive equation fitting to the reduced η-$\dot{\gamma}$ data for the temperature-, pressure-, and density-invariant master curves.

Parameter	η_0^*	η_∞^*	λ^*	a	n
Temperature invariant	1.0	0.0	0.142	0.53	0.10
Pressure invariant	1.0	0.0	0.217	0.53	0.20
Density invariant	1.0	0.0	1.151	0.53	0.58

density by the magnitude of λ^* and n parameters, is concluded: density effect > pressure effect > temperature effect. Whether dealing with "qualitative observation of flow curves" or "quantitative comparison of fitting parameters mentioned above," such results lead us to assure that the sequence of substantially affecting variations in η-$\dot{\gamma}$ flow curves is expressly addressed as follows: density, pressure, and temperature effects.

C. Normal stress differences and coefficients for shear shinning

Shear thinning not only presents in the viscosity-shear-rate (η-$\dot{\gamma}$) relationship but also its characteristic behavior results in variations in first and second normal stress coefficients (ψ_1 and ψ_2) along shear rates. Early NEMD studies of Barker *et al.*,[7] Davis *et al.*,[67] and Chynoweth *et al.*[49] have been performed to compute ψ_1 and ψ_2 values for alkane molecules. Recently, for short-chain PE, Moore *et al.*[22] examined the NEMD results of ψ_1 and ψ_2 compared with the reptation dynamic theory of the Doi–Edwards model,[46] which predicted $\psi_1 \propto \dot{\gamma}^{-2}$ and $-\psi_2 \propto \dot{\gamma}^{-2.5}$ for the entangled polymer dynamics, as $\dot{\gamma} \to \infty$. The variations in the ψ_1-$\dot{\gamma}$ and $-\psi_2$-$\dot{\gamma}$ data with molecular length have been mostly reported,[20,21,26,34,43,44,47] while Jabbarzadeh *et al.*[25] and Bosko *et al.*[26] discussed in detail that the degree of branching of molecules influences the ψ_1-$\dot{\gamma}$ and $-\psi_2$-$\dot{\gamma}$ curves. In particular, Bosko *et al.*[34] further revealed the polymer blending and polymeric solutions dependence on the ψ_1 and ψ_2 value. In spite of the large number of literatures, those studies mentioned above are limited to the investigations of molecular structure dependence on normal stress coefficients. It is regretful that little information has been made available regarding which thermodynamic state is directly relative to normal stress coefficients.

The major aim here is to analyze the variations in the dependence of normal stress differences and coefficients on shear rate, including N_1-$\dot{\gamma}$, $-N_2$-$\dot{\gamma}$, ψ_1-$\dot{\gamma}$, and $-\psi_2$-$\dot{\gamma}$, as well as the minus ratio of normal stress coefficients, $-\psi_2/\psi_1$-$\dot{\gamma}$; the discussions of these properties at different temperatures, pressures, and densities are addressed analytically. Significantly, the slope of shear thinning of ψ_1-$\dot{\gamma}$ and $-\psi_2$-$\dot{\gamma}$ curves obeys the power-law model to observe how the rate of shear thinning changes. In addition, *a* CT *point*, which undergoes in the dramatic variations in $-\psi_2/\psi_1$-$\dot{\gamma}$ curves, is found obviously.

1. Variations with temperature

The N_1 and ψ_1 versus $\dot{\gamma}$ for different temperatures of 300–500 K are shown in Fig. 6, where *NPT*-NEMD simulations were performed at a constant pressure of 250 MPa. Note that solid symbols indicate N_1 related to the left axis, while open symbols indicate ψ_1 related to the right axis. On the one hand, at $\dot{\gamma} < 1 \times 10^{11.5}$ s^{-1}, the ψ_1 value decreases with increasing shear rate and with increasing temperature. Surprisingly, at $\dot{\gamma} > 1 \times 10^{11.5}$ s^{-1}, the ψ_1-$\dot{\gamma}$ curves at different temperatures closely match each other. This result should be concluded virtually the $\dot{\gamma}$ independence of ψ_1.

Overall, regarding the changes in $-\psi_2$ and $-N_2$ values with shear rate and temperature, Fig. 7 is similar to the features mentioned above of ψ_1-$\dot{\gamma}$ curves in Fig. 6. Expectedly,

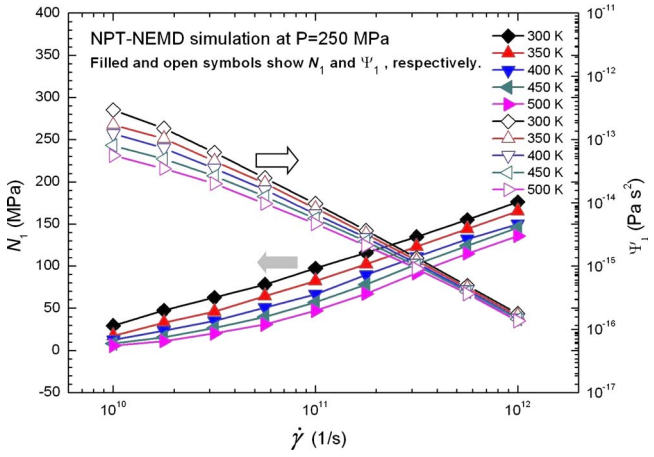

FIG. 6. (Color online) Shear-rate $\dot{\gamma}$ dependence of the first stress difference N_1 (left axis) and coefficient ψ_1 (right axis) for *n*-hexadecane at 250 MPa and varying temperatures between 300 and 500 K as obtained from *NPT*-NEMD simulation. Filled and open symbols above show N_1 and ψ_1, respectively.

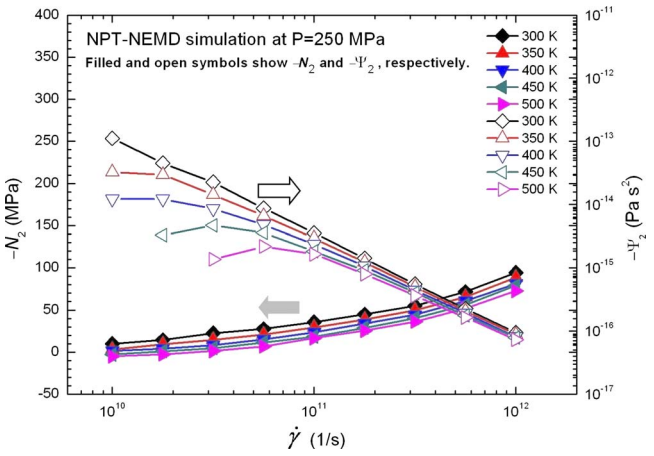

FIG. 7. (Color online) Shear-rate $\dot{\gamma}$ dependence of the minus second stress difference $-N_2$ (left axis) and coefficient $-\psi_2$ (right axis) for *n*-hexadecane at 250 MPa and varying temperatures between 300 and 500 K as obtained from *NPT*-NEMD simulation. Note that filled and open symbols above show $-N_2$ and $-\psi_2$, respectively.

This article is copyrighted as indicated in the article. Reuse of AIP content is subject to the terms at: http://scitation.aip.org/termsconditions. Downloaded to IP: 140.113.38.11 On: Wed, 30 Apr 2014 06:13:54

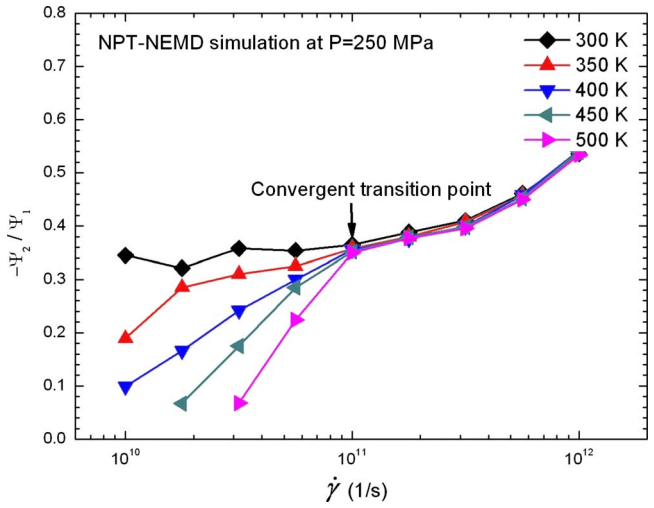

FIG. 8. (Color online) Shear-rate $\dot{\gamma}$ dependence of the minus ratio of the second to first normal stress coefficient $-\psi_2/\psi_1$ for *n*-hexadecane at 250 MPa and varying temperatures between 300 and 500 K as obtained from *NPT*-NEMD simulation.

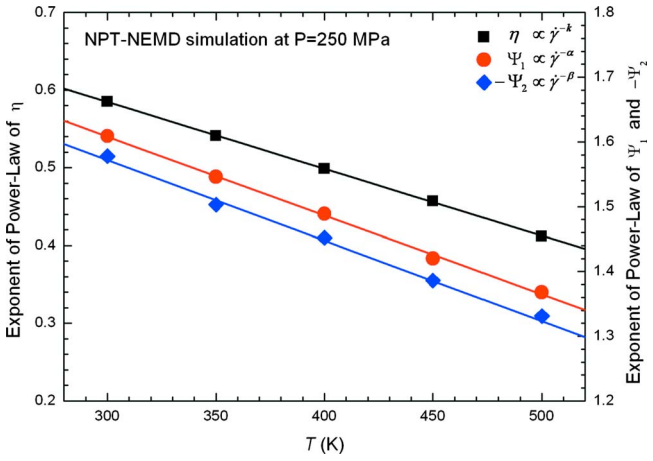

FIG. 9. (Color online) Temperature T dependence of exponents k, α, and β in shear thinning behavior of the viscosity η (left axis), first stress coefficient ψ_1, and minus second stress coefficient $-\psi_2$ (right axis) given by $\eta \propto \dot{\gamma}^{-k}$, $\psi_1 \propto \dot{\gamma}^{-\alpha}$, and $-\psi_2 \propto \dot{\gamma}^{-\beta}$ for *n*-hexadecane at 250 MPa as obtained from *NPT*-NEMD simulation in the high shear-rate range, respectively. The drawn lines are fit to the data. The square, circle, and diamond symbols above show results for η, ψ_1, and $-\psi_2$, respectively.

$-\psi_2$-$\dot{\gamma}$ curves at $\dot{\gamma} > 1 \times 10^{11.5}$ s^{-1} also closely match each other, while the $-\psi_2$-$\dot{\gamma}$ curves start separating at $\dot{\gamma} < 1 \times 10^{11.5}$ s^{-1}. In addition, the $-\psi_2$ values also decrease with increasing shear rates and with increasing temperatures. Unexpectedly, within a narrow shear-rate range of about $1 \times 10^{10.0} - 1 \times 10^{11.0}$ s^{-1}, an analogous first-Newtonian plateau of $-\psi_2$-$\dot{\gamma}$ curves is inspected for 350–500 K; this feature usually appears in rheological experiments.[37] The NEMD results of Kröger *et al.*[43] and Daivis[77] discussed the first-Newtonian plateau of ψ_1-$\dot{\gamma}$ and $-\psi_2$-$\dot{\gamma}$ curves under the zero-shear-rate limit, namely, $\psi_{1,0}$ and $-\psi_{2,0}$, respectively.

On the other hand, N_1 and $-N_2$ values increase with shear rate, while they decrease correspondingly with rising temperatures; additionally, at low shear rates, both values gradually tend toward near zero. Because thermodynamic fluctuation at low shear rates results in large statistical uncertainty, N_2 values in the present study are small positive and decay to close zero so that $-\psi_2$ values are negative, not to be shown in Fig. 7, which is due to on the logarithmic coordinates. Consequently, overall N_1 and N_2 values decrease to approximate zero with decreasing shear rates. This tendency is apparently observed in the NEMD studies of Xu *et al.*[44] and Jabbarzadeh *et al.*[25] In the other words, as both N_1 and N_2 values are almost equal to zero, the fluid approaches the Newtonian fluidic behavior.[38]

As shown in Figs. 6 and 7, the ψ_1-$\dot{\gamma}$ and $-\psi_2$-$\dot{\gamma}$ curves are nearly a linear function on the logarithmic coordinate and therefore are simply described by the power-law models, $\psi_1 \propto \dot{\gamma}^{-\alpha}$ and $-\psi_2 \propto \dot{\gamma}^{-\beta}$, where α and β are the power-law model's exponent of ψ_1 and $-\psi_2$ variables, respectively; then, these exponents at different temperatures can be obtained in Table II. In NEMD studies of *n*-butane (C_4H_{10}) and *n*-decane ($C_{10}H_{22}$) fluids, Edberg *et al.*[6] revealed that ψ_1 and $-\psi_2$ values are proportional to $\dot{\gamma}^{-1.5}$. Thereby, our predicted exponent values α and β are roughly reasonable as inspected in Table II.

Proceeding to Fig. 8, a CT point, which indicates that all curves converge together at a transition location of $\dot{\gamma} \approx 1 \times 10^{11.0}$ s^{-1}, is evidently found. After the CT point of $\dot{\gamma} > 1 \times 10^{11.0}$ s^{-1}, $-\psi_2/\psi_1$-$\dot{\gamma}$ curves matching each other is similar to ψ_1-$\dot{\gamma}$ and $-\psi_2$-$\dot{\gamma}$ curves in Figs. 6 and 7, respectively. In addition to our earlier study,[17] for high shear rates of $\dot{\gamma} > 1 \times 10^{11.5}$ s^{-1}, η-$\dot{\gamma}$ curves at different temperature nearly match each other. In summary, we suggest that at high shear rates rheological properties including η, ψ_1, $-\psi_2$, and $-\psi_2/\psi_1$ virtually do not depend on temperature. In passing, NEMD studies of Guo *et al.*[45] also presented such a result mentioned above for the η-$\dot{\gamma}$ curves of perfluoropolyether at high shear rates.

In contrast, before the CT point of $\dot{\gamma} < 1 \times 10^{11.0}$ s^{-1}, we notice that only at the lower temperature of 300 K the $-\psi_2/\psi_1$ ratio does remain approximately constant; and at other temperatures, the $-\psi_2/\psi_1$ ratio falls as temperature rises. As a whole, the $-\psi_2/\psi_1$ ratio increases with shear rate that is in accordance with the previous NEMD study of Daivis *et al.*,[8] who presented the comparative rheological properties of branched and linear alkanes. Nevertheless, the existence of this CT point should be attributed to the nonequilibrium state density being close to the equilibrium state density. The location of CT point is unexpectedly inspected at $\dot{\gamma} \approx 1 \times 10^{11.0}$ s^{-1} and is also near to the location of transient point for the shear dilatancy behavior, which happens at about $1 \times 10^{11.0}$ s^{-1} as referring to our earlier study.[17]

To describe the rate of shear thinning, we have arranged three exponents k, α, and β in Table II for $\eta \propto \dot{\gamma}^{-k}$, $\psi_1 \propto \dot{\gamma}^{-\alpha}$, and $-\psi_2 \propto \dot{\gamma}^{-\beta}$, respectively. As a result, the viscosity's k value is rather smaller than the normal stress coefficients' α and β values. In Fig. 9, the exponents depending on temperature are shown together in both left and right axes, which are related to viscosity and normal stress coefficients, respectively. Significantly, the rate of shear thinning *linearly* declines with increasing temperature.

Lastly, the related NEMD researches regarding power-law model's exponent are mentioned briefly below. In a *heterogeneous* shear flow field of *n*-hexadecane molecules un-

This article is copyrighted as indicated in the article. Reuse of AIP content is subject to the terms at: http://scitation.aip.org/termsconditions. Downloaded to IP: 140.113.38.11 On: Wed, 30 Apr 2014 06:13:54

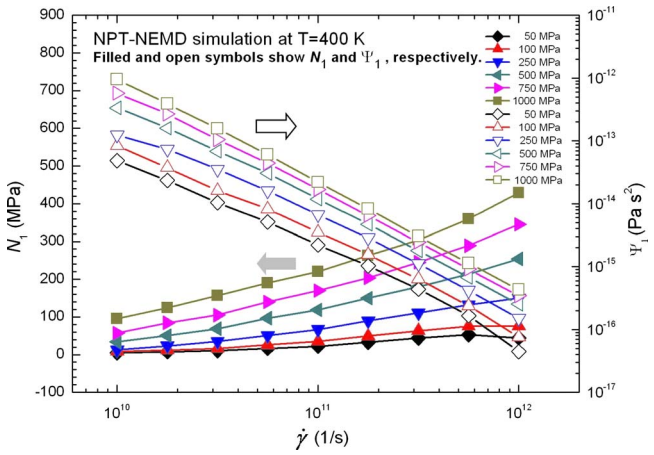

FIG. 10. (Color online) Shear-rate $\dot{\gamma}$ dependence of the first stress difference N_1 (left axis) and coefficient ψ_1 (right axis) for *n*-hexadecane at 400 K and varying pressures between 50 and 1000 MPa as obtained from *NPT*-NEMD simulation. Note that filled and open symbols above show N_1 and ψ_1, respectively.

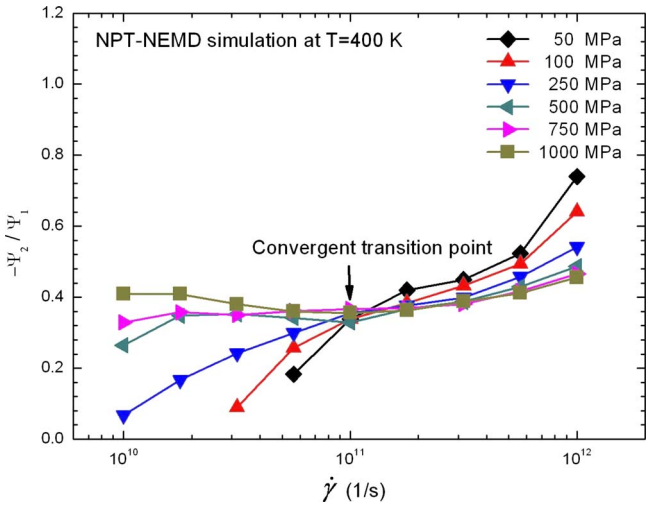

FIG. 12. (Color online) Shear-rate $\dot{\gamma}$ dependence of the minus ratio of the second to first normal stress coefficient $-\psi_2/\psi_1$ for *n*-hexadecane at 400 K and varying pressures between 50 and 1000 MPa as obtained from *NPT*-NEMD simulation.

der constant temperature and density conditions, Jabbarzadeh *et al.*[54] offered that as film thickness increased, the k value decreased for $\eta \propto \dot{\gamma}^{-k}$. For linear molecular chains, the findings of Kröger *et al.*[43] and Bosko *et al.*[26] resulted in which the α and β values increase with molecular lengths for $\psi_1 \propto \dot{\gamma}^{-\alpha}$ and $-\psi_2 \propto \dot{\gamma}^{-\beta}$, respectively. In addition, for dendrimers, Bosko *et al.*[34] further reported that the change in α and β values with increasing the degree of branching of molecules is *not obvious*.

2. Variations with pressure

Over a broad pressure of 50–1000 MPa, the changes in ψ_1 and $-\psi_2$ with $\dot{\gamma}$ are illustrated in Figs. 10 and 11, respectively, as *NPT*-NEMD simulations have been performed at a constant temperature of 400 K. With increasing shear rates, the variations in ψ_1 and $-\psi_2$ values in Figs. 10 and 11 are almost similar to those in Figs. 6 and 7. As the shear thinning characteristic is also observed in Figs. 10 and 11, the ψ_1-$\dot{\gamma}$ and $-\psi_2$-$\dot{\gamma}$ relationships are easily fitted by the power-law

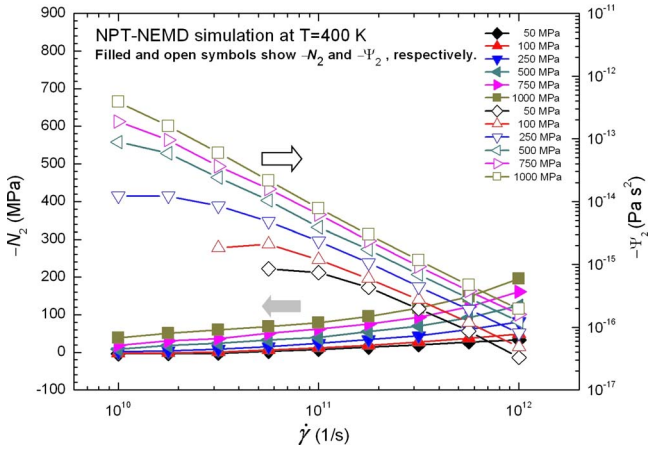

FIG. 11. (Color online) Shear-rate $\dot{\gamma}$ dependence of the minus second stress difference $-N_2$ (left axis) and coefficient $-\psi_2$ (right axis) for *n*-hexadecane at 400 K and varying pressures between 50 and 1000 MPa as obtained from NPT-NEMD simulation. Filled and open symbols above show $-N_2$ and $-\psi_2$, respectively.

model; their exponents, α and β, are listed in Table III. Additionally, as the pressure increases, it is evident that the ψ_1 and $-\psi_2$ values increase correspondingly while both exponents α and β also increase.

Only at lower pressures of below 250 MPa, the $-\psi_2$-$\dot{\gamma}$ curves in Fig. 11 possess a similar first-Newtonian plateau characteristic. Returning to Fig. 7, at higher temperatures of 350–500 K, this first-Newtonian plateau of $-\psi_2$-$\dot{\gamma}$ curves is also found. Figures 10 and 11 show that at lower pressures of 50–250 MPa, both N_1 and $-N_2$ values *rapidly converge* near to zero with decreasing shear rate; at higher pressures of over 250 MPa, it is clear that both values *gradually decay* to zero. Therefore, this result indicates that the fluidic behavior approximates Newtonian fluid especially at low shear rates.

The change in $-\psi_2/\psi_1$-$\dot{\gamma}$ curves with pressure is shown in Fig. 12, while the CT point is observed at $\dot{\gamma} \approx 1 \times 10^{11.0}$ s^{-1} again. Notice that the CT point of the $-\psi_2/\psi_1$-$\dot{\gamma}$ curves obtained at different pressures in Fig. 12 is similar to that at different temperatures in Fig. 8. Overall, the $-\psi_2/\psi_1$ ratio increases with shear rate. Especially for the higher pressure approaching to over 250 MPa, after the CT point of $\dot{\gamma} > 1 \times 10^{11.0}$ s^{-1}, the $-\psi_2/\psi_1$ ratio does not vary with increasing $\dot{\gamma}$ and all $-\psi_2/\psi_1$-$\dot{\gamma}$ curves almost match each other. In contrast to before the CT point of $\dot{\gamma} < 1 \times 10^{11.0}$ s^{-1}, at higher pressures, the change in the $-\psi_2/\psi_1$ ratio is *not obvious*. In addition, at over and below shear rates of the CT point, the variations in the $-\psi_2/\psi_1$ ratio with pressure are fortuitously inverse.

Referring to Sec. III C 1, all exponents are listed in Table III for $\eta \propto \dot{\gamma}^{-k}$, $\psi_1 \propto \dot{\gamma}^{-\alpha}$, and $-\psi_2 \propto \dot{\gamma}^{-\beta}$. As a result, these exponents increase with pressure, where α and $\beta > k$. In Fig. 13, three *intersections* are inspected respectively by two straight lines fitting to the data and their common location is found at about 320 MPa. In our earlier study,[17] notably, this intersections has been once shown in the η-P curve under constant temperature and shear-rate conditions of 400 K and $1 \times 10^{12.0}$ s^{-1}. Thus, a wide pressure region should result in the existence of the intersections regarding the

This article is copyrighted as indicated in the article. Reuse of AIP content is subject to the terms at: http://scitation.aip.org/termsconditions. Downloaded to IP: 140.113.38.11 On: Wed, 30 Apr 2014 06:13:54

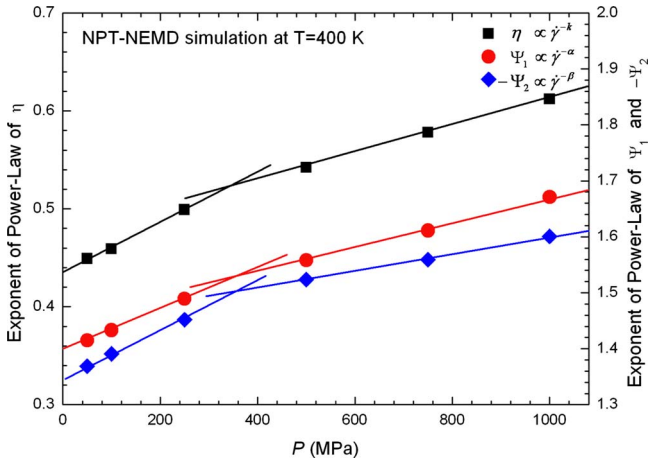

FIG. 13. (Color online) Pressure P dependence of exponents k, α, and β in shear thinning behavior of the viscosity η (left axis), first stress coefficient ψ_1, and minus second stress coefficient $-\psi_2$ (right axis) given by $\eta \propto \dot{\gamma}^{-k}$, $\psi_1 \propto \dot{\gamma}^{-\alpha}$, and $-\psi_2 \propto \dot{\gamma}^{-\beta}$ for n-hexadecane at 400 K as obtained from NPT-NEMD simulation in the high shear-rate range, respectively. The drawn lines are fit to the data. The square, circle, and diamond symbols above show results for η, ψ_1, and $-\psi_2$, respectively.

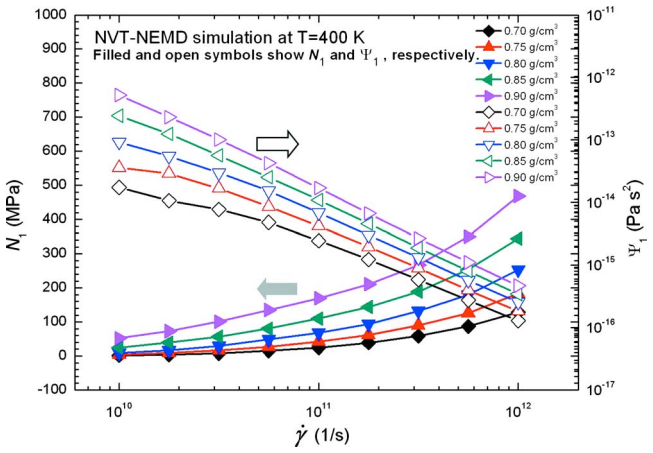

FIG. 14. (Color online) Shear-rate $\dot{\gamma}$ dependence of the first stress difference N_1 (left axis) and coefficient ψ_1 (right axis) for n-hexadecane at 400 K and varying densities between 0.70 and 0.90 g/cm^3 as obtained from NVT-NEMD simulation. Note that filled and open symbols above show N_1 and ψ_1, respectively.

variation in rheological properties with pressure. In addition, the variation in the exponent along different pressures is opposite to that along different temperatures, as seen in Figs. 9 and 13.

It is worth mentioning that the NEMD study of Bosko *et al.*[26] also finds an intersection in the k-M curve for *linear molecules*, where M is molecular weight; while *branched molecules* have the same molecular weight region with linear molecules, no intersection was observed. It is well known that the η_0-M curve in a wide molecular weight range possesses a *crossover* point from $\eta_0 \propto M^1$ to $\eta_0 \propto M^{3.4}$,[21,41] where η_0 is zero-shear-rate viscosity. In the present study, therefore, the intersections of k-P, α-P, and β-P plots should be associated with an intersection of the k-M curve and a crossover of the η_0-M curve. Because the power-law model's exponents over "a wide pressure region" are somewhat analogous to over "a wide molecular weight region," we suggest cautiously that the variation in exponents by the effect of pressure may be similar to the effect of molecular weight.

3. Variations with density

Figures 14 and 15 depict the ψ_1 and $-\psi_2$ variations along shear rates at a constant temperature of 400 K and different densities of 0.70–0.9 g/cm^3, respectively. Expectedly, at higher shear rates, the shear thinning feature appearing at the ψ_1-$\dot{\gamma}$ and $-\psi_2$-$\dot{\gamma}$ curves can be effortlessly described by $\psi_1 \propto \dot{\gamma}^{-\alpha}$ and $-\psi_2 \propto \dot{\gamma}^{-\beta}$, respectively. Their exponents α and β with respect to the density are also summarized in Table IV. As a result, ψ_1 and $-\psi_2$ values increase with density and a tendency to the variation in N_1 and N_2 values shows to reduce rapidly to near zero with declining shear rate. At low shear rates, however, the fluidic behavior is almost of Newtonian fluid.

Dramatically, the CT point at $\dot{\gamma} \approx 1 \times 10^{10.75}$ s^{-1} in Fig. 16 exhibits that all $-\psi_2/\psi_1$-$\dot{\gamma}$ curves at different densities collect together; then, this result could be associated with shear dilatancy of NVT-NEMD simulation, which has a transient points occurring within the interval between about $1 \times 10^{10.5}$ and $1 \times 10^{11.0}$ s^{-1} as referring to our earlier study.[17] Since the CT point's location in Fig. 16 is roughly close to the transient points of shear dilatancy, one may deduce that this CT point is related to shear dilatancy. As mentioned above in Figs. 8 and 12, this suggestion has also explained the CT point occurring at $-\psi_2/\psi_1$-$\dot{\gamma}$ curve for different temperatures and pressures, respectively.

As shown in Fig. 16, after or before the CT point, the overall $-\psi_2/\psi_1$ ratio always increases with the shear rate. Unexpectedly, before the CT point of $\dot{\gamma} < 1 \times 10^{10.75}$ s^{-1}, the $-\psi_2/\psi_1$ ratio at the lowest density of 0.70 g/cm^3 actually declines with increasing shear rate. This observation is approximate to the result of Khara *et al.*,[10] which regards the NEMD simulations of n-hexadecane fluid at 373 K and 0.725 g/cm^3. Notably, in the liquid-vapor coexistence curve of our previous study,[17] n-hexadecane molecules at 400 K and over 0.65 g/cm^3 are of course the complete liquid state; in contrast to below 0.65 g/cm^3, the fluid exhibits the coex-

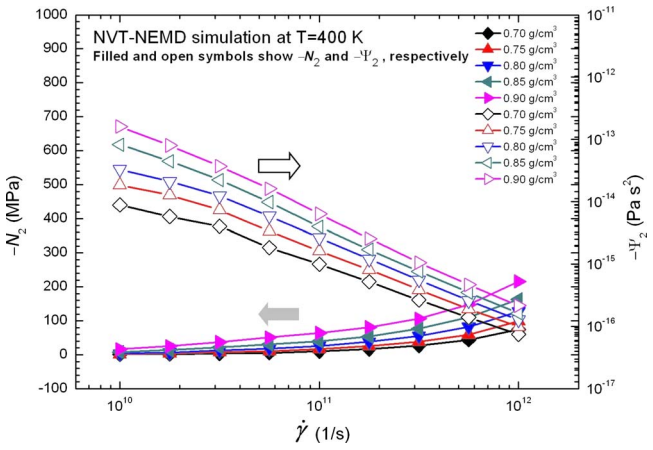

FIG. 15. (Color online) Shear-rate $\dot{\gamma}$ dependence of the minus second stress difference $-N_2$ (left axis) and coefficient $-\psi_2$ (right axis) for n-hexadecane at 400 K and varying densities between 0.70 and 0.90 g/cm^3 as obtained from NVT-NEMD simulation. Filled and open symbols above show $-N_2$ and $-\psi_2$, respectively.

This article is copyrighted as indicated in the article. Reuse of AIP content is subject to the terms at: http://scitation.aip.org/termsconditions. Downloaded to IP: 140.113.38.11 On: Wed, 30 Apr 2014 06:13:54

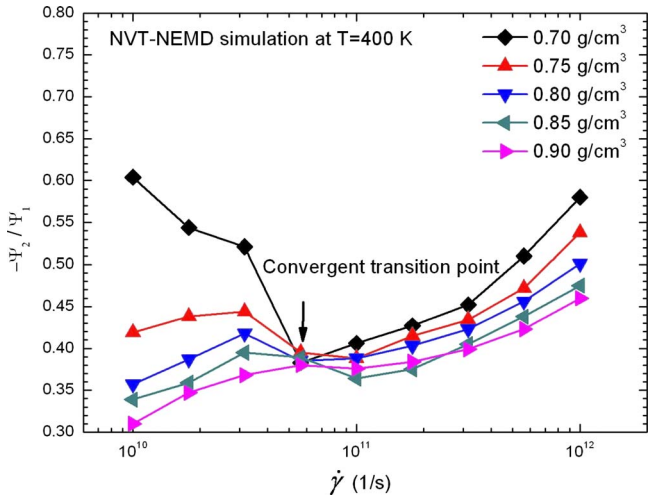

FIG. 16. (Color online) Shear-rate $\dot{\gamma}$ dependence of the minus ratio of the second to first normal stress coefficient $-\psi_2/\psi_1$ for *n*-hexadecane at 400 K and varying densities between 0.70 and 0.90 g/cm^3 as obtained from *NVT*-NEMD simulation.

istence of liquid and vapor states. Thereby, we propose that this individual occurrence may be made due to the fluidic state approaching the coexistence of liquid and vapor states. In addition, our result with respect to the $\dot{\gamma}$ dependence of $-\psi_2/\psi_1$ at different densities is in rough agreement with the study of Khara *et al.*[10] and the related rheological treatise.[37]

Finally, three exponents k, α, and β at different densities are organized in Table IV, where α and $\beta > k$. Proceeding to Fig. 17, the rate of shear thinning increases linearly with density. As a consequence, the parallel of the rate of shear thinning is drawn between pressure and density effects. Comparably, the variation in the rate of shear thinning with temperature is just opposite to that with pressure and density. In summary, the tendency to vary of these three exponents is the same no matter how temperature, pressure, and density effects change, as illustrated in Figs. 9, 13, and 17. More

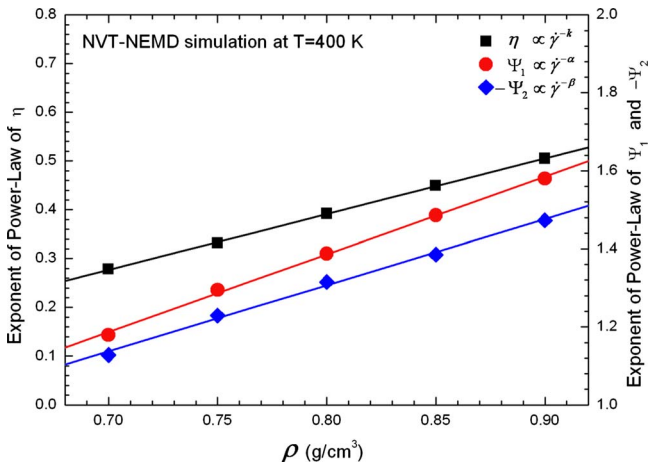

FIG. 17. (Color online) Density ρ dependence of exponents k, α, and β in shear thinning behavior of the viscosity η (left axis), first stress coefficient ψ_1, and minus second stress coefficient $-\psi_2$ (right axis) given by $\eta \propto \dot{\gamma}^{-k}$, $\psi_1 \propto \dot{\gamma}^{-\alpha}$, and $-\psi_2 \propto \dot{\gamma}^{-\beta}$ for *n*-hexadecane at 400 K as obtained from *NVT*-NEMD simulation in the high shear-rate range, respectively. The drawn lines are fit to the data. The square, circle, and diamond symbols above show results for η, ψ_1, and $-\psi_2$, respectively.

importantly, we found that the qualitative variations in the degree of shear thinning is fortuitously contrary to that of the degree of shear dilatancy, which results are referred to our earlier study.[17]

IV. CONCLUSIONS

A wealth of noteworthy information concerning rheological properties of liquid *n*-hexadecane has allowed us to investigate via NEMD simulations, including both constant volume and constant pressure systems with the coarse-grained molecular potential model. Under different temperature (T), pressure (P), and density (ρ) conditions, we have performed the reasonable comparison of rheological properties with related NEMD simulations, experimental, and theoretical studies.

Viscosity is one of the standard material parameters in the discussions of rheological properties under steady shear. The viscosity-shear-rate (η-$\dot{\gamma}$) relationship containing two important features—the zero-shear-rate viscosity (η_0) in the first-Newtonian plateau and the slope of shear thinning in the non-Newtonian region—is clearly observed. Thus, the overall η-$\dot{\gamma}$ curves can be well described by the Carreau–Yasuda constitutive equation to further gain the extrapolative η_0 value.

Rouse's rotational relaxation time (τ_R) can be assessed by the η_0 value, while critical shear rate ($\dot{\gamma}_c$) is nearly the inverse of τ_R, $\dot{\gamma}_c \approx \tau_R^{-1}$. Most importantly, by adopting η_0 and $\dot{\gamma}_c$ values we successfully normalize all η-$\dot{\gamma}$ curves to obtain separately temperature-, pressure-, and density-invariant master curves, which are additionally formulated by the Carreau–Yasuda model. As a result, whether dealing with qualitative observations of the η-$\dot{\gamma}$ curves or quantitative comparison of fitting parameters, the order of affecting the variation's sensitivity of the η-$\dot{\gamma}$ curves is addressed as follows: the strongest is density effect, the second is pressure effect, and the weakest, correspondingly, is temperature effect.

Another important material parameters, responses to first and second normal stress coefficients (ψ_1 and ψ_2), are always discussed to understand shear thinning under steady shear. In the present study, the overall observations represent that the η, ψ_1, and $-\psi_2$ values expectably decrease with rising temperature; whereas the pressure and density are enhanced, the η, ψ_1, and $-\psi_2$ values obviously increase. In particular, for high shear rates of $\dot{\gamma} > 1 \times 10^{11.5}$ s^{-1}, η, ψ_1, $-\psi_2$, and $-\psi_2/\psi_1$ almost do not depend on temperature. Shear thinning, which indicates that the η, ψ_1, and $-\psi_2$ values are linearly related to $\dot{\gamma}$ on the logarithmic coordinate, can be described via the power-law model, $\eta \propto \dot{\gamma}^{-k}$, $\psi_1 \propto \dot{\gamma}^{-\alpha}$, and $-\psi_2 \propto \dot{\gamma}^{-\beta}$, respectively. Consequently, the tendency to vary of the rate of shear thinning is the same no matter how the temperature, pressure, and density effects change. The rate of shear thinning falls with rising temperature, while it increases with increasing density or pressure.

Surprisingly, we inspect that the tendency to vary of the degree of shear thinning in rheology is *contrary* to the degree of shear dilatancy in thermodynamics. Notably, at low shear rates, first and second normal stress differences (N_1 and N_2)

This article is copyrighted as indicated in the article. Reuse of AIP content is subject to the terms at: http://scitation.aip.org/termsconditions. Downloaded to IP: 140.113.38.11 On: Wed, 30 Apr 2014 06:13:54

decay to near zero, $N_1 \approx 0$ and $N_2 \approx 0$, while the fluid's nonequilibrium states are close to equilibrium ones, $P(\dot{\gamma}) \approx P(\dot{\gamma}=0)$ or $\rho(\dot{\gamma}) \approx \rho(\dot{\gamma}=0)$. Thereby, such findings demonstrate that the fluid at the nonequilibrium thermodynamics states and very low shear rates should approach the Newtonian fluidic characteristics.

Moreover, whether related to the temperature and pressure effects, a CT point, which indicates that all $-\psi_2/\psi_1$ curves almost collect together, obviously exhibit in the vicinity of $\dot{\gamma} \approx 1 \times 10^{11.0}$ s^{-1}. In addition to the density effect, the CT point occurs at $\dot{\gamma} \approx 1 \times 10^{10.75}$ s^{-1}. This point's location is approximate to the transient point of shear dilatancy, which appears in the interval between about $1 \times 10^{10.5}$ and $1 \times 10^{11.0}$ s^{-1}. Thus, the above simple notion leads us to propose that the existence of the CT point should be indirectly related to shear dilatancy.

As a whole, the $-\psi_2/\psi_1$ ratios increase with shear rate. Especially at lower shear rates of below the CT point for the lower temperature of 300 K or the higher pressure of over 500 MPa, the $-\psi_2/\psi_1$ ratios practically remain constant with increasing shear rates. As the changes in the $-\psi_2/\psi_1$ ratio with respect to the temperature, pressure, and density are dramatic, these significant outcomes, which have a connection with the CT point, are summarized analytically in three points below.

(1) For different temperatures: After the CT point, $-\psi_2/\psi_1$ ratio is *not* related to temperature; before the CT point, $-\psi_2/\psi_1$ ratio decreases with rising temperature.
(2) For different pressures: After the CT point, $-\psi_2/\psi_1$ ratio decreases as pressure increases; in contrast, before the CT point, $-\psi_2/\psi_1$ ratio increases with pressure.
(3) For different densities: After or before the CT point, the overall $-\psi_2/\psi_1$ ratio decreases with increasing density.

In the near future, NEMD studies will also be evidently interested in broadening our understanding with respect to the shear dilatancy and shear thinning behaviors as related to the molecular perspective, including configuration, conformation, orientation, relaxation time, and internal energy.

ACKNOWLEDGMENTS

We are very grateful to the reviewers for their constructive comments. We thank the National Science Council of the Republic of China (Grant No. NSC97-2221-E-007-033) and CoreTech System Co., Ltd (Moldex3D) for financial support.

[1] M. P. Allen and D. J. Tildesley, *Computer Simulation of Liquid* (Clarendon, Oxford, 1989).
[2] R. J. Sadus, *Molecular Simulation of Fluids* (Elsevier, New York, 1999).
[3] D. J. Evans and G. P. Morriss, *Statistical Mechanics of Nonequilibrium Liquids* (Cambridge University Press, Cambridge, 2008).
[4] D. M. Heyes, J. Chem. Soc., Faraday Trans. 2 **82**, 1365 (1986).
[5] D. J. Evans and G. P. Morriss, Phys. Rev. Lett. **56**, 2172 (1986).
[6] R. Edberg, G. P. Morriss, and D. J. Evans, J. Chem. Phys. **86**, 4555 (1987).
[7] A. Berker, S. Chynoweth, U. C. Klomp, and Y. Michopoulos, J. Chem. Soc., Faraday Trans. **88**, 1719 (1992).
[8] P. J. Daivis, D. J. Evans, and G. P. Morriss, J. Chem. Phys. **97**, 616 (1992).
[9] S. Chynoweth and Y. Michopoulos, Mol. Phys. **81**, 133 (1994).
[10] R. Khare, J. de Pablo, and A. Yethiraj, J. Chem. Phys. **107**, 6956 (1997).
[11] L. I. Kioupis and E. J. Maginn, J. Phys. Chem. B **104**, 7774 (2000).
[12] J. D. Moore, S. T. Cui, H. D. Cochran, and P. T. Cummings, J. Chem. Phys. **113**, 8833 (2000).
[13] S. Bair, C. McCabe, and P. T. Cummings, Phys. Rev. Lett. **88**, 058302 (2002).
[14] C. McCabe, C. W. Manke, and P. T. Cummings, J. Chem. Phys. **116**, 3339 (2002).
[15] Y. Yang, T. A. Pakkanen, and R. L. Rowley, Int. J. Thermophys. **23**, 1441 (2002).
[16] G. Pan and C. McCabe, J. Chem. Phys. **125**, 194527 (2006).
[17] H.-C. Tseng, J.-S. Wu, and R.-Y. Chang, J. Chem. Phys. **129**, 014502 (2008).
[18] J. Petravic and J. Delhommelle, J. Chem. Phys. **122**, 234509 (2005).
[19] D. R. Wheeler and R. L. Rowley, Mol. Phys. **94**, 555 (1998).
[20] T. Aoyagi and M. Doi, Comput. Theor. Polym. Sci. **10**, 317 (2000).
[21] M. Kröger and S. Hess, Phys. Rev. Lett. **85**, 1128 (2000).
[22] J. D. Moore, S. T. Cui, H. D. Cochran, and P. T. Cummings, J. Non-Newtonian Fluid Mech. **93**, 83 (2000).
[23] J. D. Moore, S. T. Cui, H. D. Cochran, and P. T. Cummings, J. Non-Newtonian Fluid Mech. **93**, 101 (2000).
[24] P. J. Daivis, M. L. Matin, and B. D. Todd, J. Non-Newtonian Fluid Mech. **111**, 1 (2003).
[25] A. Jabbarzadeh, J. D. Atkinson, and R. I. Tanner, Macromolecules **36**, 5020 (2003).
[26] J. T. Bosko, B. D. Todd, and R. J. Sadus, J. Chem. Phys. **121**, 12050 (2004).
[27] J. M. Kim, D. J. Keffer, M. Kröger, and B. J. Edwards, J. Non-Newtonian Fluid Mech. **152**, 168 (2008).
[28] S. Balasubramanian, C. J. Mundy, and M. L. Klein, J. Chem. Phys. **105**, 11190 (1996).
[29] J. Delhommelle and J. Petravic, J. Chem. Phys. **118**, 2783 (2003).
[30] N. Galamba, C. A. Nieto de Castro, and J. F. Ely, J. Chem. Phys. **122**, 224501 (2005).
[31] L. I. Kioupis and E. J. Maginn, Chem. Eng. J. **74**, 129 (1999).
[32] Y.-R. Jeng, C.-C. Chen, and S.-H. Shyu, J. Appl. Phys. **95**, 8450 (2004).
[33] H. Zhang and J. F. Ely, Fluid Phase Equilib. **217**, 111 (2004).
[34] J. T. Bosko, B. D. Todd, and R. J. Sadus, J. Chem. Phys. **123**, 034905 (2005).
[35] T. Kairn, P. J. Daivis, I. Ivanov, and S. N. Bhattacharya, J. Chem. Phys. **123**, 194905 (2005).
[36] H.-C. Tseng, J.-S. Wu, and R.-Y. Chang, "Linear viscoelasticity and thermorheological simplicity of *n*-hexadecane under sinusoidal oscillatory shear via non-equilibrium molecular dynamics simulations," J. Chem. Phys. (submitted).
[37] R. B. Bird, R. C. Armstrong, and O. Hassager, *Fluid Mechanics, Dynamics of Polymeric Liquids*, 2nd ed. (Wiley-Interscience, New York, 1987), Vol. 1.
[38] J. M. Dealy and K. F. Wissbrun, *Melt Rheology and its Role in Plastics Processing* (Kluwer, Dordrecht, 1999).
[39] F. A. Morrison, *Understanding Rheology* (Oxford University Press, New York, 2001).
[40] R. L. Ballman, Nature (London) **202**, 288 (1964).
[41] J. D. Ferry, *Viscoelastic Properties of Polymers*, 3rd ed. (Wiley-Interscience, New York, 1980).
[42] M. T. Shaw and W. J. MacKnight, *Introduction to Polymer Viscoelasticity*, 3rd ed. (Wiley-Interscience, Hoboken, 2005).
[43] M. Kröger, W. Loose, and S. Hess, J. Rheol. **37**, 1057 (1993).
[44] Z. Xu, J. J. de Pablo, and S. Kim, J. Chem. Phys. **102**, 5836 (1995).
[45] Q. Guo, P. S. Chung, H. Chen, and M. S. Jhon, J. Appl. Phys. **99**, 08N105 (2006).
[46] M. Doi and S. F. M. Edwards, *The Theory of Polymer Dynamics* (Clarendon, Oxford, 1986).
[47] J. T. Padding and W. J. Briels, J. Chem. Phys. **118**, 10276 (2003).
[48] D. J. Evans and G. P. Morriss, Comput. Phys. Rep. **1**, 297 (1984).
[49] S. Chynoweth, R. C. Coy, and Y. Michopoulos, Proc. Inst. Mech. Eng., Part J: J. Eng. Tribol. **209**, 243 (1995).
[50] M. G. Martin and J. I. Siepmann, J. Phys. Chem. B **102**, 2569 (1998).
[51] C. McCabe, S. Cui, P. T. Cummings, P. A. Gordon, and R. B. Saeger, J. Chem. Phys. **114**, 1887 (2001).
[52] ASME Research Committee on Lubrication, *Pressure-Viscosity Report* (American Society of Mechanical Engineers, New York, 1953), Vol. II.
[53] R. C. Reid, J. M. Prausnitz, and B. E. Poling, *The Properties of Gases and Liquids*, 4th ed. (McGraw-Hill, New York, 1987).

This article is copyrighted as indicated in the article. Reuse of AIP content is subject to the terms at: http://scitation.aip.org/termsconditions. Downloaded to IP: 140.113.38.11 On: Wed, 30 Apr 2014 06:13:54

[54] A. Jabbarzadeh, J. D. Atkinson, and R. I. Tanner, J. Non-Newtonian Fluid Mech. **77**, 53 (1998).
[55] A. Jabbarzadeh, J. D. Atkinson, and R. I. Tanner, J. Chem. Phys. **110**, 2612 (1999).
[56] A. Jabbarzadeh, J. D. Atkinson, and R. I. Tanner, Tribol. Int. **35**, 35 (2002).
[57] S. W. Bunte and H. Sun, J. Phys. Chem. B **104**, 2477 (2000).
[58] D. Rigby, H. Sun, and B. E. Eichinger, Polym. Int. **44**, 311 (1997).
[59] H.-C. Tseng, J.-S. Wu, and R.-Y. Chang, "Master curves and radial distribution functions for shear dilatancy of liquid *n*-hexadecane via nonequilibrium molecular dynamics simulations," J. Chem. Phys. (submitted).
[60] H.-C. Tseng, J.-S. Wu, and R.-Y. Chang, "Nano-contraction flows of short-chain polyethylene via molecular dynamics simulations," Mol. Simul. DOI:10.1080/08927020802651613 (in press).
[61] J. M. Haile, *Molecular Dynamics Simulation*, 2nd ed. (Wiley-Interscience, New York, 1997).
[62] D. N. J. White and M. J. Bovill, J. Chem. Soc., Perkin Trans. 2 1610 (1977).
[63] J. P. Ryckaert and A. Bellemans, Chem. Phys. Lett. **30**, 123 (1975).
[64] P. J. Flory, *Statistical Mechanics of Chain Molecules* (Hanser, Munich, 1989).
[65] The original SLLOD algorithm is denominated from the transpose of the Dolls' tensor (dyadic product of position and momenta), which is named after the Kewpie Doll by W. G. Hoover. See Refs. 3 and 48.
[66] A. W. Lees and S. F. Edwards, J. Phys. C **5**, 1921 (1972).
[67] P. J. Daivis and D. J. Evans, J. Chem. Phys. **100**, 541 (1994).
[68] J. Delhommelle and D. J. Evans, J. Chem. Phys. **115**, 43 (2001).
[69] K. P. Travis, P. J. Daivis, and D. J. Evans, J. Chem. Phys. **103**, 10638 (1995).
[70] K. P. Travis, P. J. Daivis, and D. J. Evans, J. Chem. Phys. **103**, 1109 (1995).
[71] S. A. Gupta, H. D. Cochran, and P. T. Cummings, J. Chem. Phys. **107**, 10316 (1997).
[72] D. Dowson, *Thin Films in Tribology*, Proceedings of the 19th Leeds-Lyon Symposium on Tribology (Elsevier, Amsterdam, 1993), pp. 3–12.
[73] D. Macgowan and D. M. Heyes, Mol. Simul. **1**, 277 (1988).
[74] J. H. Irving and J. G. Kirkwood, J. Chem. Phys. **18**, 817 (1950).
[75] J. E. Carpenter, J. Comput. Chem. **23**, 667 (2002).
[76] Y. Tsuchiya, H. Hasegawa, and T. Iwatsubo, J. Chem. Phys. **114**, 2484 (2001).
[77] P. J. Daivis, J. Non-Newtonian Fluid Mech. **152**, 120 (2008).

This article is copyrighted as indicated in the article. Reuse of AIP content is subject to the terms at: http://scitation.aip.org/termsconditions. Downloaded to IP: 140.113.38.11 On: Wed, 30 Apr 2014 06:13:54